# Integrated Localization and Communication for Efficient Millimeter Wave Networks

Girim Kwon<sup>®</sup>, *Member, IEEE*, Zhenyu Liu<sup>®</sup>, *Member, IEEE*, Andrea Conti<sup>®</sup>, *Fellow, IEEE*, Hyuncheol Park<sup>®</sup>, *Senior Member, IEEE*, and Moe Z. Win<sup>®</sup>, *Fellow, IEEE* 

Abstract—Integrated localization and communication (ILC) at millimeter wave (mmWave) frequencies will be a key enabler for providing accurate location information and high data rate communication in beyond fifth generation (B5G) networks. This paper proposes a transmission frame structure and a soft information (SI)-based localization algorithm for positionassisted communications. In accordance with B5G specifications, we consider multiple-input multiple-output (MIMO)-orthogonal frequency division multiplexing (OFDM) networks. Theoretical limits are also derived to serve both as performance benchmark and as input for algorithm design. The proposed method enables cooperative ILC with improved localization accuracy and enhanced communication rate simultaneously. In particular, position-assisted communication at mmWave frequencies is explored accounting for the statistical characteristics of the wireless environment. Localization accuracy and communication rate are quantified in 3rd Generation Partnership Project (3GPP) network scenarios. Results show that the SI-based localization algorithm achieves decimeter-level accuracy, approaching the theoretical limit. Moreover, the position-assisted communication can provide higher communication rate with reduced overhead compared to existing techniques, especially in scenarios with high mobility.

Index Terms—Integrated localization and communication, millimeter wave networks, MIMO, OFDM, soft information.

# I. INTRODUCTION

NTEGRATED localization and communication (ILC) is expected to play a key role for numerous applications in beyond fifth generation (B5G) wireless networks [1], [2], [3], [4], [5], [6]. These applications include autonomy [7], [8], [9], [10], [11], crowd sensing [12], [13], [14], [15], smart environments [16], [17], [18], assets tracking [19],

Manuscript received 15 February 2023; revised 27 June 2023; accepted 13 August 2023. Date of current version 22 November 2023. The fundamental research described in this paper was supported, in part, by the National Research Foundation of Korea under Grant 2021R1A6A3A14040142, by the Ministry of Science and ICT under Grant IITP-2023-RS-2023-0025991, by the Office of Naval Research under Grant N62909-22-1-2009, by the National Science Foundation under Grant CNS-2148251, and in part by federal agency and industry partners in the RINGS program. (Corresponding author: Moe Z. Win.)

Girim Kwon and Zhenyu Liu are with the Wireless Information and Network Sciences Laboratory, Massachusetts Institute of Technology, Cambridge, MA 02139 USA (e-mail: girimk@mit.edu; zliu14@mit.edu).

Andrea Conti is with the Department of Engineering and CNIT, University of Ferrara, 44122 Ferrara, Italy (e-mail: a.conti@ieee.org).

Hyuncheol Park is with the School of Electrical Engineering, Korea Advanced Institute of Science and Technology, Daejeon 34141, Republic of Korea (e-mail: hcpark@kaist.ac.kr).

Moe Z. Win is with the Laboratory for Information and Decision Systems (LIDS), Massachusetts Institute of Technology, Cambridge, MA 02139 USA (e-mail: moewin@mit.edu).

Color versions of one or more figures in this article are available at https://doi.org/10.1109/JSAC.2023.3322760.

Digital Object Identifier 10.1109/JSAC.2023.3322760

[20], [21], [22], and Internet-of-Things (IoT) [23], [24], [25], [26]. For example, ILC with decimeter-level localization accuracy and gigabit-per-second data rate will enable safe driving of connected and automated vehicles (CAVs), including lane change, collision avoidance, and indoor parking [27], [28]. To this end, cellular-based localization techniques have received attention and evolved in the standardization process [1], [3], [5], [29]. Fifth generation (5G) New Radio (NR) is expected to meet those performance requirements [1], [3], [5]. In particular, millimeter wave (mmWave) networks can enable new applications via large bandwidth exploitation, multiantenna processing, multi-node cooperation, and intelligent surface control [3], [30], [31], [32].

Although mmWave networks have been extensively investigated, most studies have focused only on communication and not on ILC [33], [34], [35], [36], [37], [38]. The design of ILC for efficient mmWave networks is crucial for sharing the spectrum and hardware between localization and communication. In particular, a suitable frame structure for ILC is needed especially for networks with multiple antennas and multiple nodes. The main challenges in designing ILC at mmWave frequencies are: to achieve high localization accuracy and high communication rate simultaneously with limited wireless resources; and to overcome the harsh propagation environments with acute pathloss, severe multi-path, and frequent blockage of line-of-sight (LOS) path.

In recent years, mmWave localization has been explored in the literature, while research on the ILC method at mmWave frequencies is still lacking. The existing works are categorized into three main streams: i) performance analysis [39], [40], [41], [42], ii) transceiver design [43], [44], [45], and iii) localization algorithm design [4], [6], [46], [47], [48], [49]. In particular, ILC methods for mmWaves have been investigated in [42] and [43] in terms of the position error bound and communication rate. Localization algorithms for mmWave networks have been designed for narrowband systems in [46], [47], and [48] and wideband systems in [4], [6], and [49]. For accurate localization in realistic mmWave environments, harsh propagation conditions (e.g., LOS blockage and multi-path scattering) should be taken into account to design localization algorithms.

Classical localization techniques relying on single-value estimates (SVEs) (e.g., range and angle estimates) may suffer from performance degradation as the SVEs are biased in the conditions with LOS blockage and multi-path scattering [50], [51], [52], [53], [54]. To overcome this drawback, the direct positioning (DP) techniques have been proposed [55], [56], [57], [58], [59]. However, they are still not robust particularly

0733-8716 © 2023 IEEE. Personal use is permitted, but republication/redistribution requires IEEE permission. See https://www.ieee.org/publications/rights/index.html for more information.

when measurements are obtained in different propagation conditions. For accurate localization in harsh mmWave environments, statistical characteristics of the measurements in different propagation conditions should be taken into account in designing localization algorithms.

To capture richer information from statistical characterization of heterogeneous measurements, soft information (SI)-based localization has been investigated [4], [6], [60], [61]. SI contains all the positional information inherent in the signal measurements as well as in the contextual data, allowing more accurate localization than the SVE-based and DP methods. In [4] and [6], the generative models learned from the SVEs and their true values have been used for SIbased localization. For a full exploitation of SI in mmWave networks, however, it is necessary to characterize the relationship between the received reference signals and the user equipment (UE) positions in realistic propagation environments. This approach allows to account for signal correlation across different frequencies of the wideband system and for cooperation among multiple gNodeBs (gNBs) in dense 5Gand-beyond mmWave networks, thus improving localization and communication performance.

The fundamental questions related to cooperative ILC for mmWave networks are: i) what frame structure can be used for accurate localization as well as high rate communication; ii) how to design efficient algorithms for ILC accounting for statistical characteristics of mmWave channel; and iii) what gain can be obtained via gNB cooperation and multiple antennas in terms of both localization accuracy and communication rate. The answers to these questions will enable development of cooperative ILC methods for mmWaves in B5G networks. The goal of this paper is to determine theoretical limits of mmWave ILC and to design methods for achieving improved localization accuracy and enhanced communication rate. We advocate position-assisted communication, via a suitable ILC frame structure, in which the positions of multiple UEs are simultaneously estimated and used for reducing communication overhead (see an illustration of ILC in Fig. 1). The key idea is to exploit the spatial reciprocity of uplink (UL) and downlink (DL) channels, as well as the correlation among different subcarriers. This enables simultaneous localization of multiple UEs based only on a short reference signal.

This paper develops a cooperative ILC method for mmWave multiple-input multiple-output (MIMO)-orthogonal frequency division multiplexing (OFDM) networks. The key contributions of this paper can be summarized as in the following:

- propose an efficient ILC frame structure for positionassisted communication by exploiting spatial reciprocity between UL and DL channels to reduce the communication overhead;
- determine the theoretical limits of localization in mmWave MIMO-OFDM networks based on the Fisher information, accounting for gNBs cooperation and signal correlation among subcarriers;
- design the SI-based localization algorithm, which approaches the theoretical performance limits by

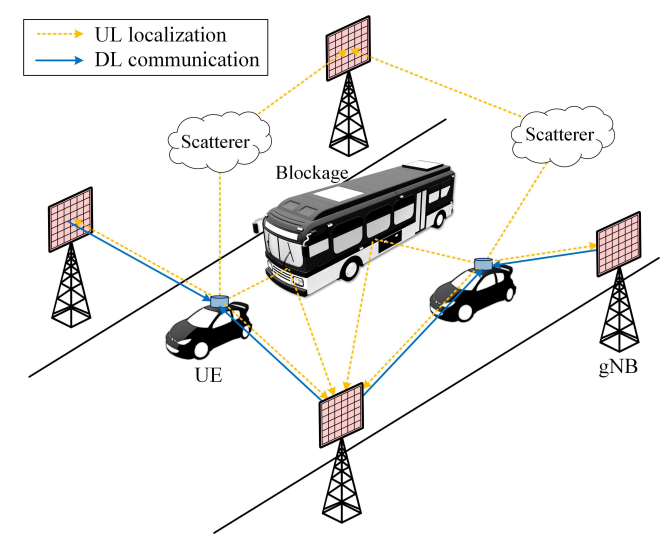


Fig. 1. An illustration of the ILC method in a network with multiple gNBs and UEs. LOS paths may be blocked by obstacles, and non-line-of-sight (NLOS) multi-path components exist randomly.

- exploiting the statistical characteristics of mmWave signals including LOS blockage and random scattering; and
- quantify the performance of the proposed ILC method in indoor and urban scenarios according to 3rd Generation Partnership Project (3GPP) specifications for mmWave networks.

The remaining sections are organized as in the following: Sec. II describes the system model of the proposed ILC method. Sec. III determines the theoretical limits of mmWave localization. Sec. IV presents the SI-based localization algorithm. Sec. V develops the position-assisted communication scheme. Sec. VI quantifies the performance of the proposed ILC method. Finally, Section VII gives our conclusions.

Notations: Random variables (RVs) are displayed in sans serif, upright fonts; their realizations in serif, italic fonts. Vectors and matrices are denoted by bold lowercase and uppercase letters, respectively. For example, a RV and its realization are denoted by x and x; a random vector and its realization are denoted by x and x; a random matrix and its realization are denoted by X and X, respectively. Sets and random sets are denoted by upright sans serif and calligraphic font, respectively. For example, a random set and its realization are denoted by X and  $\mathcal{X}$ , respectively. The m-by-n matrix of zeros is denoted by  $\mathbf{0}_{m \times n}$ ; when n = 1, the m-dimensional vector of zeros is simply denoted by  $\mathbf{0}_m$ . The m-by-m identity matrix is denoted by  $I_m$ : the subscript is removed when the dimension is clear from the context. The relation  $X\succ 0$ means that X is positive definite. The operators tr(X) and  $||X||_{\rm F}$  denote the trace and the Frobenius norm, respectively. The operations ⊗ and ⊙ denote the Kronecker product and element-wise product, respectively. The function  $f_{\mathbf{x}}(\mathbf{x}; \mathbf{a})$  and, for brevity when possible, f(x; a) denote the probability distribution function (PDF) of a continuous RV x parameterized by a;  $f_{x|y}(x|y;a)$  and, for brevity when possible, f(x|y;a)denote the PDF of x conditional on y = y parameterized by a;  $\varphi(x; \mu, \Sigma)$  denotes the PDF of a circularly-symmetric complex Gaussian (CSCG) RV  ${\bf x}$  with mean  ${m \mu}$  and covariance matrix  $\Sigma$ . The operators  $\mathbb{P}\{\cdot\}$  and  $\mathbb{E}\{\cdot\}$  denote the probability and expectation of the arguments, respectively. The Kronecker delta function is denoted by  $\delta_{i,j}$ . The imaginary unit is denoted by  $\imath$  such that  $\imath^2 = -1$ . The transpose and conjugate transpose of  $\boldsymbol{X}$  are denoted by  $\boldsymbol{X}^T$  and  $\boldsymbol{X}^\dagger$ , respectively. The real part of a complex number is denoted by  $\Re\{\cdot\}$ .

#### II. SYSTEM MODEL

This section describes the proposed ILC method, the channel model, and the signaling format.

# A. mmWave ILC With gNB Cooperation

Consider ILC in a mmWave network composed of  $N_{\rm B}$ gNBs and  $N_{\mathrm{U}}$  UEs, where each gNB and UE have  $M_{\mathrm{B}}$  and  $M_{\rm U}$  antennas, respectively. The gNBs cooperatively receive and transmit the signals for localization and communication, respectively. Consider a wideband mmWave network, where MIMO-OFDM system with K subcarriers and the subcarrier spacing  $\Delta f$  is adopted as in 3GPP NR. Fig. 1 illustrates the operation of the proposed ILC method in the network. For efficient use of the frequency band and the hardware system, a UL localization phase and a DL communication phase are incorporated as a form of ILC. The position estimates can be used not only for the DL communication but also for other location-based services in beyond 5G applications. If UEs need the position information, the position estimates can be sent via DL communication. Meanwhile, gNB cooperation is taken into account to provide accurate localization as well as high communication rate by exploiting macrodiversity. Since the communication rate may be degraded by the signaling overhead required for reference/pilot signal transmission and channel information feedback, an efficient ILC method for mmWave networks is designed based on position-assisted communication.

The proposed frame structure for mmWave ILC consists of two sequential phases as shown in Fig. 2. The goal of the first phase is to estimate the positions of the UEs at the gNBs using short UL reference signals, while the goal of the second phase is to transmit the DL pilot and data symbols by exploiting the estimated position information. In particular, distinguishable subsets of subcarriers can be allocated to UEs in the UL localization phase so that the reference signals can be transmitted simultaneously from multiple UEs. The received signals at the gNBs are used for the SI-based localization algorithm based on statistical characterization of the mmWave OFDM signals. Meanwhile, all the subcarriers are shared to all the UEs via space division multiple access in the DL communication phase. Since the position estimates can be used for determining the UE association and the transmit beamforming (BF) in DL communication based on spatial reciprocity, the overhead for DL channel estimation can be significantly reduced by estimating the beamformed channels with reduced dimensions instead of the full channel matrices. The intuition behind this idea is that the UE position can be inferred using only a subset of subcarriers as the spatial information is correlated over all the subcarriers.

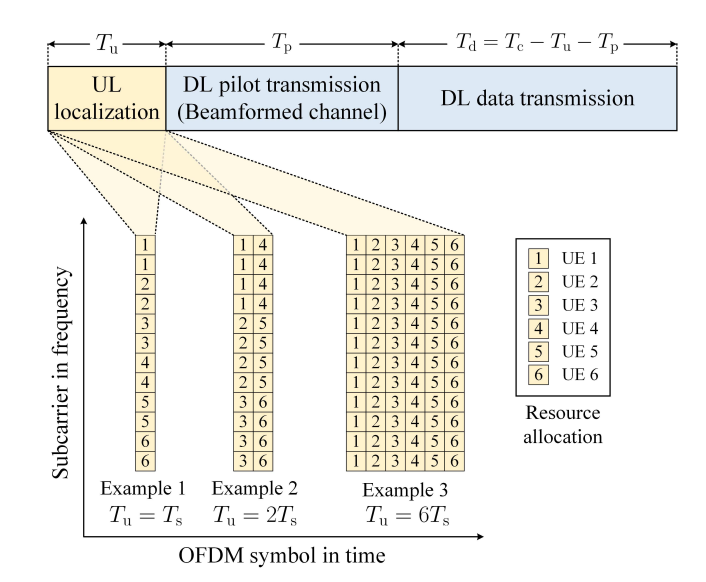


Fig. 2. Frame structure of the proposed ILC method. The UL reference signals are used for UE localization, which helps reduce the DL pilot overhead by exploiting the knowledge of the position estimates of the UEs at the gNBs. The localization accuracy and the signaling overhead have a trade-off depending on the resource allocation for UE localization. In this figure, 12 subcarriers are allocated to U=6 UEs.

#### B. Channel Model

The three-dimensional (3D) positions and orientation angles of the bth gNB are denoted by  $\boldsymbol{q}_b = [q_b^{\mathrm{x}}, q_b^{\mathrm{y}}, q_b^{\mathrm{z}}]^{\mathrm{T}}$  and  $(\varphi_b^{\mathrm{B}}, \vartheta_b^{\mathrm{B}})$ , respectively, which are known to all the gNBs. In particular,  $\varphi_b^{\mathrm{B}}$  and  $\vartheta_b^{\mathrm{B}}$  are angles with respect to the z-axis and the -x-axis, respectively. Meanwhile, the uth UE is located at an unknown position  $\boldsymbol{p}_u = [p_u^{\mathrm{x}}, p_u^{\mathrm{y}}, p_u^{\mathrm{z}}]^{\mathrm{T}}$ , which is to be estimated in the localization phase.

The UL channel from the uth UE to the bth gNB at the kth subcarrier is expressed by the matrix  $\mathbf{H}_{b,u}[k] \in \mathbb{C}^{M_{\mathrm{B}} \times M_{\mathrm{U}}}$ . For fixed  $p_u$  and  $q_b$ , the channel matrix is given by a clustered model including a probabilistic LOS path and multiple scattering clusters at random positions as follows [34], [62], [63], [64],

$$\mathbf{H}_{b,u}[k] = \mathbf{H}_{b,u}^{(0)}[k] + \sum_{i=1}^{L_{c}} \sum_{j=1}^{L_{r}} \sqrt{\varrho_{b,u}^{(i,j)}} \mathbf{H}_{b,u}^{(i,j)}[k]$$
 (1)

where  $\mathbf{H}_{b,u}^{(0)}[k]$  is the LOS component, while  $\mathbf{H}_{b,u}^{(i,j)}[k]$  is the NLOS component for the jth scattering path within the ith cluster. The numbers of scattering clusters and rays per cluster are denoted by  $L_{\rm c}$  and  $L_{\rm r}$ , respectively. The NLOS path power is normalized as  $\sum_{i=1}^{L_{\rm c}}\sum_{j=1}^{L_{\rm r}}\varrho_{b,u}^{(i,j)}=1$ . Considering probabilistic existence of the LOS path and using a single index l indicating both the LOS and NLOS paths, i.e.,  $l=0,1,\ldots,L-1$  with  $L=L_{\rm c}L_{\rm r}+1$ , the channel model in (1) can be expressed as

$$\mathbf{H}_{b,u}[k] = \chi_{b,u} \, \mathbf{H}_{b,u,0}[k] + \sum_{l=1}^{L-1} \mathbf{H}_{b,u,l}[k]$$
 (2)

where

$$\mathbf{\chi}_{b,u} = \begin{cases} 1 & \text{with probability } p_{\mathrm{L}}(r_{b,u}) \\ 0 & \text{with probability } 1 - p_{\mathrm{L}}(r_{b,u}) \end{cases}$$

$$\begin{split} \boldsymbol{H}_{b,u,0}[k] &\triangleq \sqrt{M_{\mathrm{B}} M_{\mathrm{U}} \tilde{h}_{b,u}^{(\mathrm{L})}} e^{-\imath 2\pi k \Delta f \tau_{b,u,0}} \\ &\quad \times \boldsymbol{a}_{\mathrm{B}}(\phi_{b,u,0},\theta_{b,u,0}) \, \boldsymbol{a}_{\mathrm{U}}^{\dagger} \big(\phi_{b,u,0}^{\prime},\theta_{b,u,0}^{\prime}\big) \\ \boldsymbol{\mathsf{H}}_{b,u,l}[k] &\triangleq \sqrt{\varrho_{b,u,l} M_{\mathrm{B}} M_{\mathrm{U}} \tilde{h}_{b,u}^{(\mathrm{N})}} \boldsymbol{\alpha}_{b,u,l} e^{-\imath 2\pi k \Delta f \tau_{b,u,l}} \\ &\quad \times \boldsymbol{a}_{\mathrm{B}}(\phi_{b,u,l},\theta_{b,u,l}) \, \boldsymbol{a}_{\mathrm{U}}^{\dagger} \big(\phi_{b,u,l}^{\prime},\theta_{b,u,l}^{\prime}\big) \,. \end{split}$$

In (2), the random existence of the LOS path is represented by the binary indicator  $\chi_{b,u} \in \{0,1\}$ , which follows the Bernoulli distribution with respect to the LOS probability  $p_{\rm L}(r_{b,u})$  depending on the LOS path distance  $r_{b,u}$ . The matrices  $H_{b,u,0}[k]$  and  $H_{b,u,l}[k]$  correspond to the LOS and NLOS propagation paths, respectively. The large-scale channel gains for LOS and NLOS paths are given by  $\tilde{h}_{b,u}^{(\mathrm{L})} \triangleq c_{\mathrm{L}} r_{b,u}^{-\beta_{\mathrm{L}}}$  and  $\tilde{h}_{b,u}^{(\mathrm{N})} \triangleq c_{\mathrm{N}} r_{b,u}^{-\beta_{\mathrm{N}}}$ , respectively, where  $\beta_{\mathrm{L}}$  and  $\beta_{\mathrm{N}}$  are the pathloss exponents, and  $c_{\rm L}$  and  $c_{\rm N}$  are known constants. The propagation delays for the LOS path and the lth NLOS path are denoted by  $\tau_{b,u,0}$  and  $\tau_{b,u,l}$ , respectively. In particular, the LOS path delay is given by  $\tau_{b,u,0} = r_{b,u}/c$  where c is the speed of light. The complex path gain for the lth path is denoted by the random variable  $\alpha_{b,u,l}$ , which follows the CSCG distribution with zero-mean and unit-variance. The normalized array response vector of the gNBs is denoted by  $a_{\rm B}(\phi,\theta)$  as a function of the azimuth and zenith angle-ofarrivals (AOAs) for each path. The mth element of  $a_{\rm B}(\phi,\theta)$ is given by

$$\left[\boldsymbol{a}_{\mathrm{B}}(\phi,\theta)\right]_{m} \triangleq \frac{1}{\sqrt{M_{\mathrm{B}}}} \exp\left(-\imath \boldsymbol{g}_{\mathrm{B},m}^{\mathrm{T}} \boldsymbol{k}(\phi,\theta)\right)$$

for  $m=1,2,\ldots,M_{\rm B}$ , where  $g_{{\rm B},m}$  is the relative position vector of the mth element of the antenna array of the gNB with  $g_{{\rm B},1}=0$ , and the wave vector is given by

$$\mathbf{k}(\phi, \theta) \triangleq \frac{2\pi}{\lambda_0} [\cos \phi \sin \theta, \sin \phi \sin \theta, \cos \theta]^{\mathrm{T}}$$

with the wavelength  $\lambda_{\rm c}$ . The array response vector of the UE  $a_{\rm U}(\phi,\theta)$  is similarly defined as  $a_{\rm B}(\phi,\theta)$ . The azimuth(zenith) AOAs are denoted by  $\phi_{b,u,0}(\theta_{b,u,0})$  for LOS and  $\phi_{b,u,l}(\theta_{b,u,l})$  for NLOS, respectively. Similarly, the azimuth(zenith) angle-of-departures (AODs) are denoted by  $\phi'_{b,u,0}(\theta'_{b,u,0})$  for LOS and  $\phi'_{b,u,l}(\theta'_{b,u,l})$  for NLOS, respectively. Note that the AOAs and delay of the LOS path can be expressed as functions of  $p_u$  for given  $q_b$  and  $(\varphi_b^{\rm B}, \vartheta_b^{\rm B})$  by the following coordinate transformation

$$\phi_{b,u,0} = \tan^{-1} \left( \mathring{p}_{b,u,y} / \mathring{p}_{b,u,x} \right)$$
 (3a)

$$\theta_{b,u,0} = \pi - \cos^{-1} \left( \mathring{p}_{b,u,z} / || \mathring{p}_{b,u}|| \right)$$
 (3b)

$$\tau_{b,u,0} = \frac{r_{b,u}}{c} = \|\mathbf{p}_u - \mathbf{q}_b\|/c$$
(3c)

where the rotated position vector is defined as [41]

$$\mathring{\boldsymbol{p}}_{b,u} \triangleq \boldsymbol{K}^{\mathrm{T}}(\varphi_b^{\mathrm{B}}, \vartheta_b^{\mathrm{B}})(\boldsymbol{p}_u - \boldsymbol{q}_b) = [\mathring{p}_{b,u,x}, \mathring{p}_{b,u,y}, \mathring{p}_{b,u,z}]^{\mathrm{T}}$$
(4)

with the rotation matrix

$$\boldsymbol{K}(\phi,\theta) \triangleq \begin{bmatrix} \cos \phi & -\sin \phi \cos \theta & -\sin \phi \sin \theta \\ \sin \phi & \cos \phi \cos \theta & \cos \phi \sin \theta \\ 0 & -\sin \theta & \cos \theta \end{bmatrix}. \quad (5)$$

The DL channel from the uth UE to the bth gNB at the kth subcarrier is expressed based on the spatial reciprocity by the matrix  $\mathbf{H}'_{b,u}[k] \in \mathbb{C}^{M_{\mathrm{U}} \times M_{\mathrm{B}}}$  with similar notations to (2) as

$$\mathbf{H}'_{b,u}[k] = \chi_{b,u} \, \mathbf{H}'_{b,u,0}[k] + \sum_{l=1}^{L-1} \mathbf{H}'_{b,u,l}[k]$$
 (6)

where

$$\begin{split} \boldsymbol{H}_{b,u,0}'[k] &\triangleq \sqrt{M_{\mathrm{B}} M_{\mathrm{U}} \tilde{h}_{b,u}^{(\mathrm{L})}} e^{-\imath 2\pi k \Delta f \tau_{b,u,0}} \\ &\quad \times \boldsymbol{a}_{\mathrm{U}} \left( \phi_{b,u,0}', \theta_{b,u,0}' \right) \boldsymbol{a}_{\mathrm{B}}^{\dagger} (\phi_{b,u,0}, \theta_{b,u,0}) \\ \boldsymbol{H}_{b,u,l}'[k] &\triangleq \sqrt{\varrho_{b,u,l} M_{\mathrm{B}} M_{\mathrm{U}} \tilde{h}_{b,u}^{(\mathrm{N})}} \boldsymbol{\alpha}_{b,u,l}' e^{-\imath 2\pi k \Delta f \boldsymbol{\tau}_{b,u,l}} \\ &\quad \times \boldsymbol{a}_{\mathrm{U}} \left( \phi_{b,u,l}', \boldsymbol{\theta}_{b,u,l}' \right) \boldsymbol{a}_{\mathrm{B}}^{\dagger} (\phi_{b,u,l}, \boldsymbol{\theta}_{b,u,l}) \,. \end{split}$$

The AOAs and AODs in (6) are the same with the AODs and AOAs of the UL channels, respectively. The complex path gain for the lth path is denoted by  $\alpha'_{b,u,l}$ , which follows the CSCG distribution with zero-mean and unit-variance.

## C. Signaling Format

In the UL localization phase, multiple UEs simultaneously transmit a common reference symbol s using distinguishable subsets of subcarriers to the gNBs for UE localization. Since the UEs have no prior information about the channels or relative positions of the gNBs, the reference symbol of each UE is transmitted through a single antenna element with the omnidirectional radiation pattern instead of using BF weights. In this case, the transmit BF vector of the UEs is expressed as  $e_1 \triangleq [1,0,0,\ldots,0]^T$  with length  $M_U$ . The reference symbol is received at all the gNBs. For a given symbol time of interest, the received signal at the kth subcarrier of the kth gNB from the kth UE can be expressed as

$$\begin{aligned} \mathbf{y}_{b,u}[k] &= \sqrt{P_{\rm t}} \mathbf{H}_{b,u}[k] \mathbf{e}_1 s + \mathbf{n}_{b,u}[k] \\ &= \sqrt{P_{\rm t}} \mathbf{\chi}_{b,u} \mathbf{h}_{b,u,0}[k] s + \sum_{l=1}^{L-1} \sqrt{P_{\rm t}} \mathbf{h}_{b,u,l}[k] s + \mathbf{n}_{b,u}[k] \end{aligned} \tag{7}$$

with

$$\begin{split} & \boldsymbol{h}_{b,u,0}[k] \triangleq \sqrt{M_{\mathrm{B}} \tilde{h}_{b,u}^{(\mathrm{L})}} e^{-\imath 2\pi k \Delta f \tau_{b,u,0}} \boldsymbol{a}_{\mathrm{B}}(\phi_{b,u,0},\theta_{b,u,0}) \\ & \mathbf{h}_{b,u,l}[k] \triangleq \sqrt{\varrho_{b,u,l} M_{\mathrm{B}} \tilde{h}_{b,u}^{(\mathrm{N})}} \boldsymbol{\alpha}_{b,u,l} e^{-\imath 2\pi k \Delta f \boldsymbol{\tau}_{b,u,l}} \boldsymbol{a}_{\mathrm{B}}(\phi_{b,u,l},\boldsymbol{\theta}_{b,u,l}) \end{split}$$

where  $k \in \mathcal{K}_u \subseteq \{1,2,\ldots,K\}$  and  $\mathcal{K}_u \cap \mathcal{K}_j = \emptyset$  for  $j \neq u$ . The subset  $\mathcal{K}_u$  can be chosen depending on the required localization accuracy and the number of UEs. In particular, a larger size of  $\mathcal{K}_u$  can be chosen for achieving a higher localization accuracy.  $P_t$  is the transmit power of the UE. The UL reference symbol is assumed to be a unit scalar, i.e., s=1. The noise vector  $\mathbf{n}_{b,u}[k]$  follows the CSCG distribution, i.e.,  $\mathcal{CN}(\mathbf{0}_{M_{\mathrm{B}}}, P_{\mathrm{n}}\mathbf{I}_{M_{\mathrm{B}}})$ , where  $P_{\mathrm{n}}$  is the noise power at the gNB.

In the DL communication phase, the gNBs transmit pilot symbols for channel estimation and data symbols for information transmission. In the DL pilot transmission period, a subset of gNBs  $\mathcal{B}_u \subseteq \{1,2,\ldots,N_{\mathrm{B}}\}$  is associated with the uth UE based on the results of the UL localization. Then the BF matrix  $\mathbf{F}_b \triangleq [\mathbf{f}_{b,u}, \forall u \in \mathcal{U}_b] \in \mathbb{C}^{M_{\mathrm{B}} \times |\mathcal{U}_b|}, \forall b = 1,2,\ldots,N_{\mathrm{B}}$  is used at all the subcarriers to allow a low complexity channel

acquisition at the UEs [35], [65]. The set  $\mathcal{U}_b$  includes the UEs associated with the bth gNB. In addition, we rely on the same BF matrix for both pilot and data transmissions to reduce the pilot overhead and feedback overhead. In particular, for each u, the gNBs in  $\mathcal{B}_u$  simultaneously transmit the known pilot symbol using each BF vector  $\mathbf{f}_{b,u} \in \mathbb{C}^{M_{\mathrm{B}}}$ . The details of the UE association and BF design will be explained in Sec. V. In the DL data transmission period, gNBs cooperatively transmit the data symbols to the UEs for given effective channels without the need of channel state information (CSI) feedback. The uth UE detects the transmitted symbol as

$$\mathsf{y}_u'[k] = \boldsymbol{w}_u^{\dagger} \sum_{b=1}^{N_{\mathrm{B}}} \sqrt{\frac{P_{\mathrm{t}}'}{|\mathcal{U}_b|}} \boldsymbol{H}_{b,u}'[k] \boldsymbol{F}_b \mathsf{d}_b[k] + \boldsymbol{w}_u^{\dagger} \mathsf{n}_u'[k] \quad (8)$$

where  $\boldsymbol{w}_u \in \mathbb{C}^{M_{\mathrm{U}}}$  is the receive BF vector, and  $P_{\mathrm{t}}'$  is the transmit power of the gNB. The data symbol vector is denoted by  $\mathbf{d}_b[k] = [\mathbf{s}_j'[k], j \in \mathcal{U}_b]^{\mathrm{T}}$ , where  $\mathbf{s}_j'[k]$  is the data symbol for the jth UE. This satisfies  $\mathbb{E}\{\mathbf{d}_b[k](\mathbf{d}_b[m])^{\dagger}\} = \frac{1}{|\mathcal{U}_b|}\delta_{k,m}\boldsymbol{I}_{|\mathcal{U}_b|}$ . The BF matrix  $\boldsymbol{F}_b$  is normalized so that  $\|\boldsymbol{F}_b\|_{\mathrm{F}}^2 = |\mathcal{U}_b|$ . The noise vector follows  $\mathbf{n}_u'[k] \sim \mathcal{CN}(\mathbf{0}_{M_{\mathrm{U}}}, P_{\mathrm{n}}'\boldsymbol{I}_{M_{\mathrm{U}}})$  with the noise power  $P_{\mathrm{n}}'$  at the UE.

#### III. THEORETICAL LIMIT OF MMWAVE LOCALIZATION

In this section, the theoretical limit of localization accuracy in OFDM-based mmWave MIMO networks is determined based on the Fisher information. For notational simplicity, the set of subcarrier indices allocated to the uth UE is denoted by  $\mathcal{K}_u = \{1, 2, \dots, K\}$ .

#### A. Probability Distribution of Received Signal in UL

To determine the theoretical limit of localization in terms of the Fisher information, we first derive the conditional probability distribution of the received signals at the gNBs. This result will also be used in designing the proposed localization algorithm in Sec. IV.

From (2) and (7), it can be seen that the signals at different subcarriers are correlated as the parameters  $\chi_{b,u}, \alpha_{b,u,l}, \tau_{b,u,0}, \tau_{b,u,l}, \phi_{b,u,0}, \phi_{b,u,l}, \theta_{b,u,0}$ , and  $\theta_{b,u,l}$  affect all the subcarriers. Accounting for this, we derive the joint distribution of the random vectors  $\mathbf{y}_{b,u}[k], k = 1, 2, \dots, K$  for the given set of the channel parameters defined as

$$S_{b,u} \triangleq \{ \chi_{b,u}, \tau_{b,u,l}, \phi_{b,u,l}, \theta_{b,u,l} : l = 1, 2, \dots, L - 1 \}.$$
 (9)

Define the vector  $\bar{\mathbf{y}}_{b,u}[k]$  as the concatenation of the received signals at the bth gNB from the uth UE on subcarriers  $k, k-1, \ldots, 1$ , i.e.,

$$\bar{\mathbf{y}}_{b,u}[k] \triangleq \left[\mathbf{y}_{b,u}^{\mathrm{T}}[k], \mathbf{y}_{b,u}^{\mathrm{T}}[k-1], \dots, \mathbf{y}_{b,u}^{\mathrm{T}}[1]\right]^{\mathrm{T}}.$$
 (10)

The next lemma shows that  $\bar{\mathbf{y}}_{b,u}[K]$  follows the multivariate Gaussian distribution for the given  $S_{b,u}$  and  $p_u$ .

Lemma 1: The PDF of  $\bar{\mathbf{y}}_{b,u}[K]$  for the given  $\mathcal{S}_{b,u}$  and  $p_u$  is given by

$$f_{\bar{\mathbf{y}}_{b,u}[K]|\mathbf{S}_{b,u}}(\bar{\mathbf{y}}_{b,u}[K]|\mathcal{S}_{b,u}; \mathbf{p}_{u})$$

$$= \varphi(\bar{\mathbf{y}}_{b,u}[K]; \bar{\boldsymbol{\mu}}_{b,u}^{(\chi_{b,u})}[K], \bar{\boldsymbol{\Sigma}}_{b,u}[K]) \quad (11)$$

where

$$\bar{\boldsymbol{\mu}}_{b,u}^{(\chi_{b,u})}[k] = \chi_{b,u} \sqrt{M_{\rm B} P_{\rm t} \tilde{h}_{b,u}^{(\rm L)}} \left[ \rho_{b,u,0}^{(-k)}, \rho_{b,u,0}^{(-k+1)}, \cdots, \rho_{b,u,0}^{(-1)} \right]^{\rm T} \\ \otimes \boldsymbol{a}_{\rm B}(\phi_{b,u,0}, \theta_{b,u,0})$$

$$\bar{\boldsymbol{\Sigma}}_{b,u}[k] = M_{\mathrm{B}} P_{\mathrm{t}} \tilde{\boldsymbol{h}}_{b,u}^{(\mathrm{N})} \sum_{l=1}^{L-1} \varrho_{b,u,l} \boldsymbol{R}_{b,u,l}[k] \otimes \boldsymbol{A}_{b,u,l} + P_{\mathrm{n}} \boldsymbol{I}$$

with  $\rho_{b,u,l}^{(n)} \triangleq e^{i2\pi n\Delta f \tau_{b,u,l}}$ . The matrix  $\mathbf{R}_{b,u,l}[k] \in \mathbb{C}^{k \times k}$  accounts for the correlation among the subcarriers, in which the element on the nth row and the mth column is defined as  $\left[\mathbf{R}_{b,u,l}[k]\right]_{n,m} \triangleq \rho_{b,u,l}^{(n-m)}$ . The matrix  $\mathbf{A}_{b,u,l}$  is defined as

$$\mathbf{A}_{b,u,l} \triangleq \mathbf{a}_{\mathrm{B}}(\phi_{b,u,l}, \theta_{b,u,l}) \, \mathbf{a}_{\mathrm{B}}^{\dagger}(\phi_{b,u,l}, \theta_{b,u,l}) \,. \tag{12}$$

The next proposition shows that the PDF in (11) can be factorized into the PDFs of K correlated random vectors.

Proposition 1: The PDF of  $\bar{\mathbf{y}}_{b,u}[K]$  for the given  $\mathcal{S}_{b,u}$  and  $p_u$  is factorized into the PDFs of  $\mathbf{y}_{b,u}[k]$  for the given  $\bar{\mathbf{y}}_{b,u}[k-1]$  and  $\mathcal{S}_{b,u}$  for  $k=1,2,\ldots,K$  as

$$f_{\bar{\mathbf{y}}_{b,u}[K]|S_{b,u}}(\bar{\mathbf{y}}_{b,u}[K]|S_{b,u}; \mathbf{p}_{u})$$

$$= \prod_{k=1}^{K} \varphi(\mathbf{y}_{b,u}[k]; \hat{\boldsymbol{\mu}}_{b,u}^{(\chi_{b,u})}[k], \hat{\boldsymbol{\Sigma}}_{b,u}[k])$$
(13)

where

$$\hat{\boldsymbol{\mu}}_{b,u}^{(\chi_{b,u})}[k] = \boldsymbol{\mu}_{b,u}^{(\chi_{b,u})}[k] + \bar{\boldsymbol{\Sigma}}_{b,u}^{(1,2)}[k] (\bar{\boldsymbol{\Sigma}}_{b,u}^{(2,2)}[k])^{-1} \times (\bar{\boldsymbol{y}}_{b,u}[k-1] - \bar{\boldsymbol{\mu}}_{b,u}^{(\chi_{b,u})}[k-1])$$
(14)

$$\hat{\Sigma}_{b,u}[k] = \bar{\Sigma}_{b,u}^{(1,1)}[k] - \bar{\Sigma}_{b,u}^{(1,2)}[k] \left(\bar{\Sigma}_{b,u}^{(2,2)}[k]\right)^{-1} \bar{\Sigma}_{b,u}^{(2,1)}[k]. \tag{15}$$

The definitions of  $\mu_{b,u}^{(\chi_{b,u})}[k]$  and  $\bar{\Sigma}_{b,u}^{(i,j)}[k]$  are given in (37) of Appendix B.

*Proof:* Refer to Appendix B. 
$$\Box$$

This result will be used for the derivation of the Fisher information matrix (FIM) of the received signals as well as the design of localization algorithm.

#### B. Bayesian Cramér-Rao Lower Bound for Position Estimate

To evaluate the localization accuracy, the mean square error (MSE) of the estimator  $\hat{\mathbf{p}}_u$  is used as the performance metric. In particular, the Miller-Chang type bound in [66] is used as a form of Bayesian Cramér-Rao lower bound (CRLB), which takes the expectation of the conditional CRLB over a random nuisance parameter. By treating the random parameters in the union set  $\mathbf{S}_u \triangleq \bigcup_{b=1}^{N_{\mathrm{B}}} \mathbf{S}_{b,u}$  as nuisance parameters, the MSE of  $\hat{\mathbf{p}}_u$  over the set of the observations, i.e.,  $\mathbf{Y}_u \triangleq \{\bar{\mathbf{y}}_{b,u}[K]: b=1,2,\ldots,N_{\mathrm{B}}\}$ , can be lower bounded as

$$\mathbb{E}_{\mathsf{Y}_u} \{ \| \widehat{\mathbf{p}}_u - \mathbf{p}_u \|^2 \} = \mathbb{E}_{\mathsf{S}_u} \Big\{ \mathbb{E}_{\mathsf{Y}_u | \mathsf{S}_u} \Big\{ \| \widehat{\mathbf{p}}_u - \mathbf{p}_u \|^2 | \mathsf{S}_u \Big\} \Big\}$$
 (16a)

$$\geqslant \mathbb{E}_{\mathsf{S}_u} \Big\{ \mathrm{tr} \Big( J^{-1} \big( p_u | \mathsf{S}_u \big) \Big) \Big\}$$
 (16b)

$$=: e_{\rm sp}^{\ell}(\boldsymbol{p}_u). \tag{16c}$$

In (16a), the law of iterated expectation is used. In (16b), the CRLB is given by using the FIM  $J(p_u|S_u)$  of the observation  $Y_u$  for given position  $p_u$  and nuisance parameter set  $S_u$ . In (16c), we define the squared position error bound (SPEB) as the CRLB for the position estimation, which is denoted

by  $e_{\mathrm{sp}}^{\ell}(\boldsymbol{p}_{u})$ . Defining  $X_{u} \triangleq \{\chi_{b,u} : b = 1, 2, \dots, N_{\mathrm{B}}\}$ and  $\mathring{\mathsf{S}}_u \triangleq \mathsf{S}_u \backslash \mathsf{X}_u = \{ \mathsf{\tau}_{b,u,l}, \varphi_{b,u,l}, \theta_{b,u,l} : b = 1, 2, \dots, N_{\mathsf{B}}, l = 1, 2, \dots, L-1 \}$ , the SPEB can be calculated as follows,

$$l = 1, 2, \dots, L - 1\}, \text{ the SPEB can be calculated as follows,}$$

$$e_{\mathrm{sp}}^{\ell}(\boldsymbol{p}_{u}) = \mathbb{E}_{\mathring{\mathsf{S}}_{u}} \Big\{ \mathbb{E}_{\mathsf{X}_{u}} \Big\{ \mathrm{tr} \Big( \boldsymbol{J}^{-1}(\boldsymbol{p}_{u} | \mathring{\mathsf{S}}_{u}, \mathsf{X}_{u} \Big) \Big) \Big| \mathring{\mathsf{S}}_{u} \Big\} \Big\}$$

$$\stackrel{(a)}{=} \mathbb{E}_{\mathring{\mathsf{S}}_{u}} \Big\{ \sum_{\mathcal{X}_{u} \in \check{\mathcal{X}}} \mathbb{P} \big\{ \mathsf{X}_{u} = \mathcal{X}_{u} \big\} \operatorname{tr} \Big( \boldsymbol{J}^{-1}(\boldsymbol{p}_{u} | \mathring{\mathsf{S}}_{u}, \mathcal{X}_{u} \Big) \Big) \Big\}$$

$$\stackrel{(b)}{\approx} \frac{1}{N_{\mathrm{s}}} \sum_{n=1}^{N_{\mathrm{s}}} \sum_{\mathcal{X}_{u} \in \check{\mathcal{X}}} \prod_{b=1}^{N_{\mathrm{B}}} (p_{\mathrm{L}}(r_{b,u}))^{\chi_{b,u}} (1 - p_{\mathrm{L}}(r_{b,u}))^{1 - \chi_{b,u}}$$

$$\times \operatorname{tr} \Big( \boldsymbol{J}^{-1}(\boldsymbol{p}_{u} | \mathring{\mathcal{S}}_{u}^{(n)}, \mathcal{X}_{u} \Big) \Big). \tag{17}$$

In (a),  $\mathbb{E}_{\mathsf{X}_u}\{\cdot\}$  is calculated using the joint LOS probability  $\mathbb{P}\{\mathsf{X}_u=\mathcal{X}_u\}$  for  $\mathcal{X}_u\in\check{\mathcal{X}}$ , where  $\check{\mathcal{X}}\triangleq\{0,1\}^{N_{\mathrm{B}}}$  is the set of all possible combinations of  $\chi_{b,u}, \forall b$ . In (b), the probability is calculated as  $\mathbb{P}\{\mathsf{X}_u=\mathcal{X}_u\}=\prod_{b=1}^{N_{\mathrm{B}}}(p_{\mathrm{L}}(r_{b,u}))^{\chi_{b,u}}(1-p_{\mathrm{L}}(r_{b,u}))^{\chi_{b,u}}$  $p_{\rm L}(r_{b,u}))^{1-\chi_{b,u}}$ . Also, we use the sample average method to evaluate the expectation with respect to  $\hat{S}_u$  because the distribution of  $\mathring{S}_u$  varies in different network environments. The number of random samples is denoted by  $N_s$ , and the nth sample of  $\mathring{S}_u$  is denoted by  $\mathring{S}_u^{(n)}$ .

The FIM  $J(p_u|\mathring{\mathcal{S}}_u^{(n)},\mathcal{X}_u)$  in (17) can be calculated as follows. Defining  $\mathcal{S}_u^{(n)} \triangleq \mathring{\mathcal{S}}_u^{(n)} \cup \mathcal{X}_u$ , the FIM  $J(p_u|\mathcal{S}_u^{(n)})$ can be expressed by a sum of  $N_{\rm B}$  FIMs of the independent observations at the gNBs as

$$J(p_u|S_u^{(n)}) = \sum_{b=1}^{N_B} J^{(b)}(p_u|S_{b,u}^{(n)})$$
 (18)

where  $\mathcal{S}_{b,u}^{(n)}$  is the subset of  $\mathcal{S}_{u}^{(n)}$  corresponding to the bth gNB. In (18),  $m{J}^{(b)}m{(p_u|\mathcal{S}_{b,u}^{(n)})}$  is the FIM of the observation  $\bar{\mathbf{y}}_{b,u}[K]$  for given  $\mathcal{S}_{b,u}^{(n)}$  at the bth gNB, which can be obtained by transforming the FIM for the channel parameters, i.e.,  $J^{(b)}(\eta_{b,u}|\mathcal{S}_{b,u}^{(n)})$ , based on the chain rule as

$$\boldsymbol{J}^{(b)}(\boldsymbol{p}_{u}|\mathcal{S}_{b,u}^{(n)}) = \frac{\partial \boldsymbol{\eta}_{b,u}^{\mathrm{T}}}{\partial \boldsymbol{p}_{u}} \boldsymbol{J}^{(b)}(\boldsymbol{\eta}_{b,u}|\mathcal{S}_{b,u}^{(n)}) \left(\frac{\partial \boldsymbol{\eta}_{b,u}^{\mathrm{T}}}{\partial \boldsymbol{p}_{u}}\right)^{\mathrm{T}}$$
(19)

where  $\eta_{b,u} \triangleq [\phi_{b,u,0}, \theta_{b,u,0}, \tau_{b,u,0}]^{\mathrm{T}}$ . In (19), the transformation matrix  $\frac{\partial \eta_{b,u}^{\mathrm{T}}}{\partial p_u} \in \mathbb{R}^{3 \times 3}$  is derived in Appendix C. The FIM  $m{J}^{(b)}ig(m{\eta}_{b,u}ig|\mathcal{S}_{b,u}^{(n)}ig)$  in (19) is defined as

$$\begin{split} & \boldsymbol{J}^{(b)} \big( \boldsymbol{\eta}_{b,u} \big| \mathcal{S}_{b,u}^{(n)} \big) \\ & \triangleq \mathbb{E} \Big\{ \frac{\partial \ln f_{\bar{\boldsymbol{y}}_{b,u}[K]} \big|_{\boldsymbol{\mathsf{S}}_{b,u}} \big( \bar{\boldsymbol{y}}_{b,u}[K] \big| \, \mathcal{S}_{b,u}^{(n)}; \boldsymbol{\eta}_{b,u} \big)}{\partial \boldsymbol{\eta}_{b,u}} \\ & \qquad \qquad \partial \ln f_{-\boldsymbol{\mathsf{T}}_{b,u}[K]} \big( \bar{\boldsymbol{\mathsf{Y}}}_{b,u}[K] \big| \, \mathcal{S}_{b,u}^{(n)}; \boldsymbol{\eta}_{b,u} \big) + \boldsymbol{\mathsf{T}}_{b,u} \boldsymbol{\mathsf{T}}_{b,u} \big) + \boldsymbol{\mathsf{T}}_{b,u} \boldsymbol{\mathsf{T}}_{$$

 $\times \left. \frac{\partial \ln f_{\bar{\mathbf{y}}_{b,u}[K]|\mathbf{S}_{b,u}} \left( \bar{\mathbf{y}}_{b,u}[K] \middle| \mathcal{S}_{b,u}^{(n)}; \boldsymbol{\eta}_{b,u} \right)}{\partial \boldsymbol{\eta}_{b.u.}^{\mathrm{T}}} \middle| \mathcal{S}_{b,u}^{(n)} \middle| \mathcal{S}_{b,u}^{(n)} \right)$ 

which can be expressed by Proposition 2.

Proposition 2: The element of the ith row and the jth column of  $\boldsymbol{J}^{(b)}(\boldsymbol{\eta}_{b,u}|\mathcal{S}_{b,u}^{(n)})$  is given by

$$\begin{split} & \left[ \boldsymbol{J}^{(b)}(\boldsymbol{\eta}_{b,u}|\mathcal{S}_{b,u}^{(n)}) \right]_{i,j} \\ & = \sum_{k=1}^{K} \operatorname{tr} \left( \left( \hat{\boldsymbol{\Sigma}}_{b,u}^{(n)}[k] \right)^{-1} \frac{\partial \hat{\boldsymbol{\Sigma}}_{b,u}^{(n)}[k]}{\partial [\boldsymbol{\eta}_{b,u}]_{i}} \left( \hat{\boldsymbol{\Sigma}}_{b,u}^{(n)}[k] \right)^{-1} \frac{\partial \hat{\boldsymbol{\Sigma}}_{b,u}^{(n)}[k]}{\partial [\boldsymbol{\eta}_{b,u}]_{j}} \right) \\ & + 2 \chi_{b,u} M_{\mathrm{B}} P_{\mathrm{t}} \tilde{h}_{b,u}^{(\mathrm{L})} \Re \left\{ \left( \dot{\boldsymbol{\mu}}_{b,u,i}^{(n)}[k] \right)^{\dagger} \left( \hat{\boldsymbol{\Sigma}}_{b,u}^{(n)}[k] \right)^{-1} \dot{\boldsymbol{\mu}}_{b,u,j}^{(n)}[k] \right\} \end{split}$$

for  $1 \leqslant i \leqslant 3, 1 \leqslant j \leqslant 3$ , where  $\hat{\mathcal{L}}_{b,u}^{(n)}[k]$  is obtained from (15) using the parameters in  $\mathcal{S}_{b,u}^{(n)}$ . The matrix  $\frac{\partial \hat{\Sigma}_{b,u}^{(n)}[k]}{\partial [\eta_{b,u}]_i}$  and the vector  $\dot{\boldsymbol{\mu}}_{b,u,i}^{(n)}[k]$  can be found in (47) and (49) of Appendix D, respectively.

*Proof:* Refer to Appendix D. From (18), (19), and Proposition 2, the SPEB in (17) is obtained.

## IV. SI-BASED LOCALIZATION ALGORITHM

As shown in Fig. 2, a UL reference symbol is sent from each UE to the gNBs for localization. In this section, an SI-based inference algorithm for UE localization is designed. In particular, the position of a UE is estimated with maximum likelihood (ML) criterion based on the expectation-maximization (EM) approach, accounting for the statistical characteristics of the received signals given in Sec. III. For notational brevity, it is assumed that the subcarriers k = 1, 2, ..., K are used for localization of the uth UE.

# A. SI-Based Localization With Approximate ML Estimation

The problem is to estimate  $p_u$  by observing the received signals at the gNBs, i.e.,  $\bar{y}_{b,u}[K] = [y_{b,u}^{\bar{\mathrm{T}}}[K], y_{b,u}^{\bar{\mathrm{T}}}[K-1], \ldots, y_{b,u}^{\bar{\mathrm{T}}}[1]]^{\mathrm{T}}$  defined in (10). Since the signal expression in (7) takes into account the statistical models of the nuisance parameters including LOS existence and multipath scattering, all the positional information can be captured by the SI associated with the measurements that coincides with the likelihood function of the position [60]. Then the position estimation problem can be formulated with ML criterion using the log-likelihood function as

$$\mathscr{P}_0: \ \hat{m{p}}_u = \mathop{\mathrm{argmax}}_{m{p}_u} \ \sum_{b=1}^{N_{\mathrm{B}}} \log f(\bar{m{y}}_{b,u}[K]; m{p}_u)$$

where  $f_{\bar{\mathbf{y}}_{b,u}[K]}(\bar{\mathbf{y}}_{b,u}[K]; \mathbf{p}_u)$  is the PDF of the observation  $\bar{\mathbf{y}}_{b,u}[K]$  for a given position  $p_u$ .

To solve the problem  $\mathscr{P}_0$ , the joint PDF of  $\bar{\mathbf{y}}_{b,u}[K]$  should be derived in a tractable form. However, it is difficult to have a useful expression of the joint PDF for the signal model based on the multi-path channel model parameterized by random scattering environment. For instance, each element of  $\mathbf{y}_{b,n}[k]$ in (7) follows the Gaussian distribution for given  $\chi_{b,u}$ , while the vector  $\mathbf{y}_{b,u}[k]$  does not follow the multivariate Gaussian distribution for given  $\chi_{b,u}$  in general. To design a tractable localization algorithm, we approximate the distribution of  $\mathbf{h}_{b,u,l}[k]$  in (7) using the Gaussian distribution with the same mean and covariance of  $\mathbf{h}_{b,u,l}[k]$ . This coincides with the fact that the sum of NLOS components follows the Gaussian distribution as L increases by the central limit theorem. From the approximation, the concatenated vector  $\bar{\mathbf{y}}_{b,u}[K]$  for given  $\chi_{b,u}$  and  $p_u$  follows the multivariate Gaussian distribution with

<sup>&</sup>lt;sup>1</sup>We observed that the performance loss caused by the Gaussian approximation is not significant when  $L_{\rm c} \geqslant 10$  with  $L_{\rm r} = 20$ , which corresponds to the parameter range for the 3GPP scenarios in [62].

the PDF given by<sup>2</sup>

$$f_{\bar{\mathbf{y}}_{b,u}[K]|\mathbf{\chi}_{b,u}}(\bar{\mathbf{y}}_{b,u}[K]|\mathbf{\chi}_{b,u}; \mathbf{p}_{u})$$

$$\approx \varphi(\bar{\mathbf{y}}_{b,u}[K]; \bar{\boldsymbol{\mu}}_{b,u}^{(\mathbf{\chi}_{b,u})}[K], \bar{\bar{\boldsymbol{\Sigma}}}_{b,u}[K])$$
(21)

$$= \prod_{k=1}^{K} \varphi \left( \boldsymbol{y}_{b,u}[k]; \tilde{\boldsymbol{\mu}}_{b,u}^{(\chi_{b,u})}[k], \tilde{\boldsymbol{\Sigma}}_{b,u}[k] \right). \tag{22}$$

In (21), the covariance matrix  $\bar{\Sigma}_{b,u}[k]$  is given by

$$\bar{\bar{\Sigma}}_{b,u}[k] = M_{\mathrm{B}} P_{\mathrm{t}} \tilde{h}_{b,u}^{(\mathrm{N})} \sum_{l=1}^{L-1} \varrho_{b,u,l} \mathbb{E} \left\{ \mathbf{R}_{b,u,l}[k] \right\} \otimes \mathbb{E} \left\{ \mathbf{A}_{b,u,l} \right\} + P_{\mathrm{n}} \mathbf{I}$$
(23)

where the expectations are numerically calculated for given distributions of  $\tau_{b,u,l}$ ,  $\varphi_{b,u,l}$ , and  $\theta_{b,u,l}$ . The factorization in (22) holds similarly to Proposition 1, where  $\tilde{\mu}_{b,u}^{(\chi_{b,u})}[k]$  and  $\tilde{\Sigma}_{b,u}[k]$  are obtained by substituting  $\bar{\Sigma}_{b,u}[k]$  for  $\bar{\Sigma}_{b,u}[k]$  in (14) and (15), respectively. Using the LOS probability, the joint PDF of  $\bar{\mathbf{y}}_{b,u}[K]$  is given by

$$f(\bar{\boldsymbol{y}}_{b,u}[K]; \boldsymbol{p}_{u})$$

$$\approx p_{L}(r_{b,u}) \prod_{k=1}^{K-1} \varphi \left( \boldsymbol{y}_{b,u}[k]; \tilde{\boldsymbol{\mu}}_{b,u}^{(1)}[k], \tilde{\boldsymbol{\Sigma}}_{b,u}[k] \right)$$

$$+ \left( 1 - p_{L}(r_{b,u}) \right) \prod_{k=1}^{K-1} \varphi \left( \boldsymbol{y}_{b,u}[k]; \tilde{\boldsymbol{\mu}}_{b,u}^{(0)}[k], \tilde{\boldsymbol{\Sigma}}_{b,u}[k] \right). (24)$$

# B. EM Algorithm for Localization

Maximization of  $\log f(\bar{y}_{b,u}[K]; p_u)$  in the problem  $\mathscr{P}_0$  is still intractable due to the sum of products formula in (24). To resolve this challenge, the expectation-maximization (EM) approach is used with the concept of *complete data*, instead of relying only on the observed data.

Define the random set  $Z_{b,u} \triangleq \{\bar{\mathbf{y}}_{b,u}[K], \chi_{b,u}\}$  as complete data, including both the observed data  $\bar{\mathbf{y}}_{b,u}[K]$  and the unobserved data  $\chi_{b,u}$ . A realization of  $Z_{b,u}$  is denoted by  $Z_{b,u}$ . Using (22), the PDF of  $Z_{b,u}$  can be expressed as

$$\begin{split} f_{\mathsf{Z}_{b,u}}(\mathcal{Z}_{b,u}; \boldsymbol{p}_{u}) &= f_{\mathsf{X}_{b,u}}(\chi_{b,u}; \boldsymbol{p}_{u}) f_{\bar{\mathbf{y}}_{b,u}[K]|\mathsf{X}_{b,u}}(\bar{\boldsymbol{y}}_{b,u}[K]|\chi_{b,u}; \boldsymbol{p}_{u}) \\ &\approx \left[ p_{\mathsf{L}}(r_{b,u}) \prod_{k=1}^{K} \varphi\left(\boldsymbol{y}_{b,u}[k]; \tilde{\boldsymbol{\mu}}_{b,u}^{(1)}[k], \tilde{\boldsymbol{\Sigma}}_{b,u}[k]\right) \right]^{\chi_{b,u}} \\ &\times \left[ \left(1 - p_{\mathsf{L}}(r_{b,u})\right) \prod_{k=1}^{K} \varphi\left(\boldsymbol{y}_{b,u}[k]; \tilde{\boldsymbol{\mu}}_{b,u}^{(0)}[k], \tilde{\boldsymbol{\Sigma}}_{b,u}[k]\right) \right]^{1 - \chi_{b,u}} \end{split}$$

where the probability mass function (PMF) of  $\chi_{b,u}$  is given by  $f_{\mathbf{X}_{b,u}}(\chi_{b,u}; \boldsymbol{p}_u) = (p_{\mathrm{L}}(r_{b,u}))^{\chi_{b,u}}(1-p_{\mathrm{L}}(r_{b,u}))^{1-\chi_{b,u}}$ .

Since the complete data cannot be fully observed, the EM algorithm maximizes the expected log-likelihood. This problem is expressed as

$$\mathscr{P}_1: \ \hat{\boldsymbol{p}}_u = \operatorname*{argmax}_{\boldsymbol{p}_u} \mathbb{E}_{\mathbf{X}_{b,u}} \Big\{ \sum_{b=1}^{N_{\mathrm{B}}} \ln f_{\mathsf{Z}_{b,u}}(\mathsf{Z}_{b,u};\boldsymbol{p}_u) \Big| \bar{\boldsymbol{y}}_{b,u}[K] \Big\}$$

 $^2$ This can be easily shown as the vector  $\bar{\mathbf{y}}_{b,u}[K]$  can be expressed by an affine transformation of the independent Gaussian RVs for given  $\chi_{b,u}$ .

where the expectation is taken over the conditional PMF  $f(\chi_{b,u}|\bar{y}_{b,u}[K];p_u)$ , which is given by

$$f(\chi_{b,u}|\bar{\boldsymbol{y}}_{b,u}[K];\boldsymbol{p}_u) = \frac{f(\mathcal{Z}_{b,u};\boldsymbol{p}_u)}{f(\bar{\boldsymbol{y}}_{b,u}[K];\boldsymbol{p}_u)}.$$
 (25)

The EM algorithm proceeds in multiple iterations including inner iterations, where each outer iteration consists of an expectation step and a maximization step. Consider the tth outer iteration of the algorithm. At the expectation step, the conditional PMF of  $\chi_{b,u}$  for given  $\bar{y}_{b,u}[K]$  is evaluated based on the position vector  $p_u^{(t-1)}$  calculated in the (t-1)th iteration. Then the expected log-likelihood of  $Z_{b,u}$  can be evaluated as a function of  $p_u$ , i.e.,

$$\ell_{u}(\boldsymbol{p}_{u};\boldsymbol{p}_{u}^{(t-1)}) \triangleq \sum_{b=1}^{N_{B}} \sum_{\chi_{b,u} \in \{0,1\}} f(\chi_{b,u} | \bar{\boldsymbol{y}}_{b,u}[K]; \boldsymbol{p}_{u}^{(t-1)}) \times \ln f(\mathcal{Z}_{b,u}; \boldsymbol{p}_{u}). \tag{26}$$

Next, at the maximization step, the position vector is updated by solving the following problem

$$\mathscr{P}_{1,a}: \ \boldsymbol{p}_{u}^{(t)} = \underset{\boldsymbol{p}_{u}}{\operatorname{argmax}} \ \ell_{u}(\boldsymbol{p}_{u}; \boldsymbol{p}_{u}^{(t-1)}).$$
 (27)

Since  $\ell_u(\boldsymbol{p}_u; \boldsymbol{p}_u^{(t-1)})$  in (26) is twice differentiable with respect to  $\boldsymbol{p}_u$ , a local optimal point of  $\mathscr{P}_{1,a}$  is found by Newton's method using both the gradient  $\nabla \ell_u = \frac{\partial \ell_u}{\partial \boldsymbol{p}_u} \in \mathbb{R}^{3\times 1}$  and Hessian matrix  $\nabla^2 \ell_u = \frac{\partial}{\partial \boldsymbol{p}_u} (\nabla \ell_u)^{\mathrm{T}} \in \mathbb{R}^{3\times 3}$ . Since the Newton's method can be used to find a local maximum value only when the Hessian matrix is negative definite, a modified ascent method is used with line search [67]. Then the position vector is updated at the sth inner iteration of the algorithm as

$$p_u^{(t,s)} = p_u^{(t,s-1)} - D_u^{(t,s)} \nabla \ell_u (p_u^{(t,s-1)}; p_u^{(t-1)})$$
 (28)

with

$$\boldsymbol{D}_{u}^{(t,s)} \triangleq \begin{cases} \left(\nabla^{2} \ell_{u}\right)^{-1} & \text{if } -\nabla^{2} \ell_{u} \succ \mathbf{0}_{3 \times 3} \\ \gamma^{(t,s)} \left(\nabla^{2} \ell_{u} - (|\lambda| + \epsilon)\boldsymbol{I}\right)^{-1} & \text{otherwise} \end{cases}$$

where the superscript (t,s) indicates the sth inner iteration of the tth outer iteration.  $\gamma^{(t,s)}$  is a step size, which is determined by the backtracking line search algorithm.  $\lambda$  is the smallest eigenvalue of  $-\nabla^2 \ell_u$ , and  $\epsilon$  is a small positive number to ensure the negative definiteness of  $D_u^{(t,s)}$ . The elements of the gradient and Hessian matrix are provided in Appendix E.

Once the inner iteration for the modified ascent algorithm converges, the position vector is updated by  $\mathbf{p}_u^{(t)} = \mathbf{p}_u^{(t,s)}$  as a solution to  $\mathcal{P}_{1,a}$  at the tth outer iteration. After the outer iteration of the EM algorithm converges, the estimated position of the uth UE is determined as  $\hat{\mathbf{p}}_u = \mathbf{p}_u^{(t)}$ . The EM algorithm for UE localization is summarized in Algorithm 1. Since the convergence of the EM sequence to either a maxima or a stationary point depends on the choice of starting point, multiple initial points are used, and the solution with the highest objective value is chosen [68].

 $^3$ The probability distributions of NLOS parameters depend on the network scenarios, e.g., Indoor, UMi, UMa, and InF, in 3GPP standard. The samples at each iteration t are drawn from the same random seed for convergence.

# Algorithm 1 EM Algorithm for Localization of the uth UE

```
Require: \{\bar{\boldsymbol{y}}_{b,u}[K], \boldsymbol{q}_b, \varphi_b^{\mathrm{B}}, \vartheta_b^{\mathrm{B}}, b = 1, 2, \dots, N_{\mathrm{B}}\}, P_{\mathrm{n}},
  1: Set \epsilon as a small positive number
  2: t \leftarrow 0
 3: Initialize p_u^{(t)} with a random position
  4: while p_u^{(t)} does not converge within max iteration do
  5:
               Calculate \{\phi_{b,u,0}, \theta_{b,u,0}, \tau_{b,u,0}, \forall b\} using (3)
 6:
               Obtain N samples of \{\tau_{b,u,l}, \varphi_{b,u,l}, \theta_{b,u,l}, \forall b, l > 0\}
  7:
                for given distributions<sup>3</sup>
               Calculate \bar{\Sigma}_{b,u}[k] in (23) by the sample mean method using the N samples in Step 7
  8:
               Calculate f(\chi_{b,u}|\bar{\mathbf{y}}_{b,u}[K]; \mathbf{p}_{u}^{(t-1)}), \forall \chi_{b,u}
  9:
                using (25)
               \boldsymbol{p}_{u}^{(t,s)} \leftarrow \boldsymbol{p}_{u}^{(t-1)}
10:
11:
               while p_u^{(t,s)} does not converge do
12:
                       s \leftarrow s + 1
13:
                       Calculate \nabla \ell_u(oldsymbol{p}_u^{(t,s-1)};oldsymbol{p}_u^{(t-1)})
14:
                       Calculate \nabla^2 \ell_u(\boldsymbol{p}_u^{(t,s-1)};\boldsymbol{p}_u^{(t-1)})
15:
                       if \nabla^2 \ell_u is negative definite then D_u^{(t,s)} \leftarrow \left(\nabla^2 \ell_u\right)^{-1}
16:
17:
18:
                               \lambda \leftarrow the smallest eigenvalue of -\nabla^2 \ell_u
19:
                              Find \gamma^{(t,s)} by backtracking line search \boldsymbol{D}_{u}^{(t,s)} \leftarrow \gamma^{(t,s)} \left( \nabla^{2} \ell_{u} - (|\lambda| + \epsilon) \boldsymbol{I} \right)^{-1}
20:
21:
22:
                      \boldsymbol{p}_{u}^{(t,s)} \leftarrow \boldsymbol{p}_{u}^{(t,s-1)} - \boldsymbol{D}_{u}^{(t,s)} \nabla \ell_{u}(\boldsymbol{p}_{u}^{(t,s-1)}; \boldsymbol{p}_{u}^{(t-1)})
23:
24
               \boldsymbol{p}_{u}^{(t)} \leftarrow \boldsymbol{p}_{u}^{(t,s)}
25:
26: end while
      \hat{m{p}}_u \leftarrow m{p}_u^{(t)}
        Return: \hat{p}_u
```

# C. Computational Complexity Analysis

The computational complexity of Algorithm 1 is examined in terms of the number of real scalar multiplications. We assume that both the matrix inversion and eigenvalue decomposition of a matrix  $X \in \mathbb{C}^{n \times n}$  require  $\mathcal{O}(n^3)$  multiplications. The complexity of Algorithm 1 is mainly determined by Step 8, Step 9, Step 14, Step 15, and Step 20. Specifically, Step 8 and Step 9 require  $\mathcal{O}(LK^3M_{\rm B}^2N_{\rm B}+NLM_{\rm B}^2N_{\rm B})$  and  $\mathcal{O}(N_{\rm B}K^4M_{\rm B}^3)$  multiplications, respectively. The complexity of calculating Step 14 and Step 15 is given by  $\mathcal{O}(N_{\rm B}K^4M_{\rm B}^3)$ , which is mainly for calculating (55). Step 20 is rarely executed, which requires the complexity of  $\mathcal{O}(J_{\rm max}N_{\rm B}K^4M_{\rm B}^3)$  in the worst case, where  $J_{\rm max}$  is the maximum number of iterations for finding an optimal step size, and  $N_{\rm B}K^4M_{\rm B}^3$  comes from calculating the objective value.

In summary, the overall complexity is given in the worst case as  $\mathcal{O}(t_{\max}(LK^3M_{\mathrm{B}}^2N_{\mathrm{B}}+NLM_{\mathrm{B}}^2N_{\mathrm{B}}+s_{\max}(J_{\max}+1)N_{\mathrm{B}}K^4M_{\mathrm{B}}^3))$ , where  $t_{\max}$  and  $s_{\max}$  are the maximum numbers of outer iteration and inner iteration, respectively. In most cases, the numbers of iterations are given as  $t_{\max}<4$ ,  $s_{\max}<6$ , and  $J_{\max}=0$  in the simulations. In particular, we will see that an indoor scenario with K=1 and  $M_{\mathrm{B}}=16$  is shown to achieve a decimeter-level accuracy.

#### V. Position-Assisted Communication

In this section, the position-assisted DL communication scheme is described. In particular, the position estimates from Algorithm 1 are used for determining the UE association  $\mathcal{U}_b$  and the BF matrix  $\mathbf{F}_b$  for all b. This strategy reduces the signaling overhead required for channel acquisition and feedback.

#### A. UE Association and Transmit Beamforming

After estimating the positions of the UEs, the gNBs transmit pilot signals so that UEs can estimate the DL channel information. The dimension of the channel that should be estimated in DL communication phase is reduced by fixing the UE association and transmit BF matrices. First, the LOS existence is detected by comparing the conditional PMF values in (25) as

$$\hat{\chi}_{b,u} = \underset{\chi_{b,u} \in \{0,1\}}{\operatorname{argmax}} f\left(\chi_{b,u} | \bar{\boldsymbol{y}}_{b,u}[K]; \hat{\boldsymbol{p}}_{u}\right). \tag{29}$$

From (29), determine the set  $U_b$  that contains the UEs having an LOS path from the *b*th gNB as

$$\mathcal{U}_b = \left\{ u : u \in \{1, 2, \dots, N_{\mathbf{U}}\} \text{ and } \hat{\chi}_{b,u} = 1 \right\}.$$
 (30)

Then  $F_b$  is constructed using  $\hat{p}_u$  and  $\mathcal{U}_b$  as

$$\mathbf{F}_b = \left[ \mathbf{f}_{b,u}, \forall u \in \mathcal{U}_b \right] \tag{31}$$

with

$$oldsymbol{f}_{b,u} = oldsymbol{a}_{\mathrm{B}}(\hat{\phi}_{b,u,0},\hat{ heta}_{b,u,0})$$

where  $\hat{\phi}_{b,u,0}$  and  $\hat{\theta}_{b,u,0}$  are obtained from  $\hat{p}_u$  using (3a) and (3b), respectively. The more accurate the position estimation, the higher communication rate can be provided as the beam direction of  $f_{b,u}$  becomes more accurate to the *u*th UE. The BF matrix in (31) is also used for data transmission without any CSI feedback from UEs. In summary, both the pilot overhead and feedback overhead are significantly reduced by using the position-assisted UE association and BF.

#### B. Receive Beamforming

The receive BF vector for the kth subcarrier at the uth UE is denoted by  $w_u[k]$ . Based on the strategy in Sec. V-A, the signal-to-interference-plus-noise ratio (SINR) for the kth subcarrier at the uth UE is expressed as

$$\gamma_{u}[k] = \frac{\left|\sum_{b \in \mathcal{B}_{u}} \sqrt{\frac{P_{t}^{\prime}}{|\mathcal{U}_{b}|}} \boldsymbol{w}_{u}^{\dagger}[k] \boldsymbol{H}_{b,u}^{\prime}[k] \boldsymbol{f}_{b,u}\right|^{2}}{\sum_{\substack{j=1, \ j \neq u}}^{N_{U}} \left|\sum_{b \in \mathcal{B}_{j}} \sqrt{\frac{P_{t}^{\prime}}{|\mathcal{U}_{b}|}} \boldsymbol{w}_{u}^{\dagger}[k] \boldsymbol{H}_{b,u}^{\prime}[k] \boldsymbol{f}_{b,j}\right|^{2} + P_{n}^{\prime} \left\|\boldsymbol{w}_{u}[k]\right\|^{2}}$$
(32)

where  $\mathcal{B}_j \triangleq \{b: b \in \{1, 2, \dots, N_{\mathrm{B}}\} \text{ and } j \in \mathcal{U}_b\}$ . If  $\mathcal{B}_u = \emptyset$ ,  $\gamma_u[k]$  is given as zero. Defining the vector  $\mathbf{h}_{u,j}^{\mathrm{eff}}[k] \triangleq \sum_{b \in \mathcal{B}_j} \sqrt{\frac{P_t'}{|\mathcal{U}_b|}} \mathbf{H}'_{b,u}[k] \mathbf{f}_{b,j}$ , (32) is expressed as

$$\gamma_{u}[k] = \frac{\boldsymbol{w}_{u}^{\dagger}[k] \left(\boldsymbol{h}_{u,u}^{\text{eff}}[k] \left(\boldsymbol{h}_{u,u}^{\text{eff}}[k]\right)^{\dagger}\right) \boldsymbol{w}_{u}[k]}{\boldsymbol{w}_{u}^{\dagger}[k] \left(\sum_{\substack{j=1,\\j\neq u}}^{N_{\text{U}}} \boldsymbol{h}_{u,j}^{\text{eff}}[k] \left(\boldsymbol{h}_{u,j}^{\text{eff}}[k]\right)^{\dagger} + P_{\text{n}}' \boldsymbol{I}\right) \boldsymbol{w}_{u}[k]}.$$
(33)

From (33),  $w_u[k]$  can be optimized to maximize the SINR by solving the problem  $\max_{w_u[k]} \gamma_u[k]$ . This is known as the generalized Rayleigh quotient problem [69], of which solution can be obtained by the generalized eigenvector of the matrix pair of  $h_{u,u}^{\rm eff}[k] \left(h_{u,u}^{\rm eff}[k]\right)^{\dagger}$  and  $\sum_{\substack{j=1\\j\neq u}}^{N_{\rm U}} h_{u,j}^{\rm eff}[k] \left(h_{u,j}^{\rm eff}[k]\right)^{\dagger} + P_{\rm n}' I$  with the largest eigenvalue. Therefore, the uth UE only needs to obtain the knowledge of the aggregated effective CSI  $h_{u,j}^{\rm eff}[k], \forall j$ . This allows for a further reduction in pilot overhead such that the gNBs in  $\mathcal{B}_u$  simultaneously transmit the pilot signal for each u. Then the required pilot overhead is  $T_{\rm p} = N_{\rm U} T_{\rm s}$ , where  $T_{\rm s}$  is the OFDM symbol period. Since  $T_{\rm p}$  is independent of  $N_{\rm B}$  or  $M_{\rm B}$ , the position-assisted communication is more beneficial in densely deployed networks with large antenna arrays.

#### C. Achievable Communication Rate

The achievable sum rate for a given channel realization is given by the following general expression

$$R = \left(1 - \frac{T_{\rm u} + T_{\rm p} + T_{\rm f}}{T_{\rm c}}\right) \sum_{k=1}^{K} \sum_{u=1}^{N_{\rm U}} \log_2 \left(1 + \gamma_u[k]\right)$$
 (34)

where  $T_{\rm u}$  is the overhead for transmitting the reference symbols for UE localization.  $T_{\rm p}$  is the pilot overhead for estimating the DL channels.  $T_{\rm f}$  is the channel feedback overhead if some information are sent from the UEs to the gNBs.  $T_{\rm c}$  is the channel coherence time as shown in Fig. 2. Note that all the UEs occupy all the subcarriers via space division multiple access in DL communications even if the subcarriers are separated to the UEs during the UL localization phase. In (34), the proposed position-assisted communication can significantly reduce  $T_{\rm p}$  and  $T_{\rm f}$  by using only a short  $T_{\rm u}$  for localization.

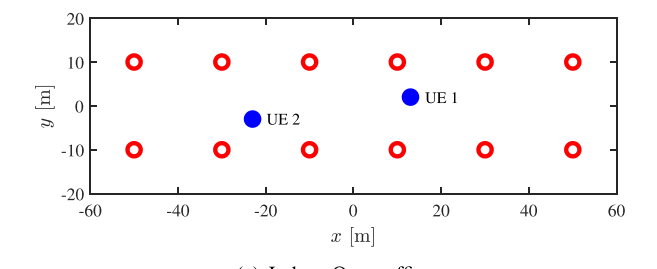
# VI. SIMULATION RESULTS

In this section, the performance of the proposed ILC method is evaluated and compared with the theoretical limit and baseline schemes.

# A. Simulation Environment

1) Network Setting: The simulations are performed for two 3GPP scenarios: Indoor-Open office and urban micro (UMi)-Street canyon [3], [62], as shown in Fig. 3. The specific parameters and models for channel realizations depend on the scenarios (see Table I). The performances are averaged over 300 channel realizations. The uniform planar arrays (UPAs) of the nodes are assumed to be placed on yz-plane by default. Then the orientation angles of the antenna arrays at the gNBs are set as follows. In Fig. 3(a),  $(\varphi_b^{\rm B}, \vartheta_b^{\rm B}) = (-90^{\rm o}, 0)$  and  $(\varphi_b^{\rm B}, \vartheta_b^{\rm B}) = (90^{\rm o}, 0)$  for the gNBs at y = 10 m and at y = -10 m, respectively. In Fig. 3(b), each gNB has three UPAs with  $(\varphi_{b,1}^{\rm B}, \vartheta_{b,1}^{\rm B}) = (30^{\rm o}, 0), (\varphi_{b,2}^{\rm B}, \vartheta_{b,2}^{\rm B}) = (-90^{\rm o}, 0),$  and  $(\varphi_{b,3}^{\rm B}, \vartheta_{b,3}^{\rm B}) = (150^{\rm o}, 0)$  to cover each  $120^{\rm o}$ -sector. For each UE, only one sector with the strongest received power of the UL signal is activated at each gNB.

2) Comparison of Localization Accuracy: The MSE of the proposed localization algorithm is verified for both indoor and outdoor scenarios. For comparison, the theoretical analysis in (17) is plotted as a lower bound of the MSE. In addition, the conventional DP scheme in [55] is compared as a baseline



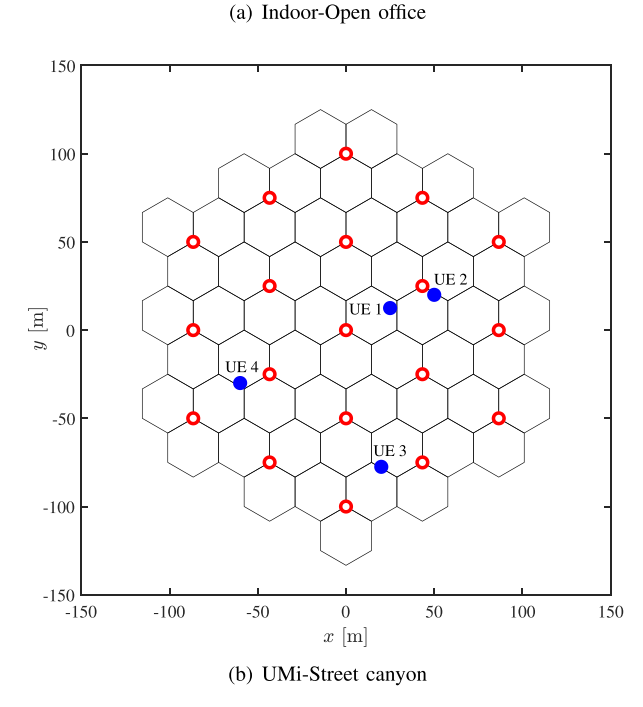


Fig. 3. 3GPP scenarios in [3] and [62]. The red rings indicate the positions of the gNBs, and the blue dots indicate the positions of the UEs. In (b), two cases are considered:  $N_{\rm B}=7$  and  $N_{\rm B}=19$ . When  $N_{\rm B}=7$ , only 7 gNBs near the origin are used.

TABLE I SIMULATION PARAMETERS

Parameter	Value	
	Indoor-Open office	UMi-Street canyon
$N_{ m B}$	12	7, 19
$N_{ m U}$	2	4
Inter-gNB distance	20 m	50 m
gNB height	3 m	10 m
UE height	1 m	1.5 m
$f_{\mathrm{c}},\Delta f$	28 GHz, 120 kHz	
$T_{ m s}$	$8.92 \mu\text{s}$ (Cyclic prefix: $0.59 \mu\text{s}$ )	
$P_{\mathrm{t}},P'_{\mathrm{t}}$	23 dBm at both gNB and UE	
LOS probability model	See Table 7.4.2-1 in [62]	
Pathloss model	See Table 7.4.1-1 in [62]	
NLOS angles and delays	See Tables in [62, Sec. 7.5]	
$L_{ m c},L_{ m r}$	19, 20	
$\varrho_{b,u}^{(i,j)}$	$1/(L_{ m c}L_{ m r})$	
Antenna array	UPA	
Noise figure	7 dB at gNB and 13 dB at UE	

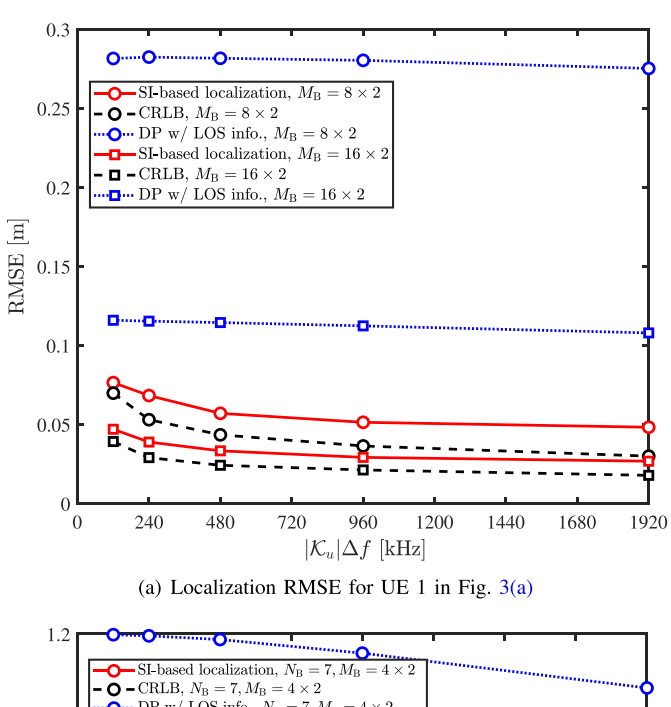
scheme. To show the ideal performance of the DP scheme, it is assumed that the LOS indicators  $\chi_{b,u}$  are perfectly known. Then the DP scheme finds the optimal position among the predefined grid on the map with respect to the least squares criterion using the received signals from the gNBs with  $\chi_{b,u}=1$ . A disadvantage of the DP is a high computational

complexity, which depends on the resolution of grid search. In our simulations, the grid resolution is set to be  $0.01\,\mathrm{m}$ . In addition, since the DP scheme is infeasible when  $\chi_{b,u}=0, \forall b$ , we discard this case for evaluating the performance of DP, while the performance of the proposed algorithm is averaged over all channel instances.

3) Comparison of Achievable Communication Rate: The achievable rate of the proposed ILC method is compared with two baseline communication schemes using (34). To focus on the effect of the estimated position information on the achievable communication rate, the following baseline schemes are considered. One is the genie-aided communication scheme having perfect knowledge of the UE positions and LOS indicators, which constitutes the transmit BF matrices using the exact LOS directions in (31). The DL transmission relies on the perfect effective CSI at the UEs without channel information feedback. The overhead terms for this scheme are given by  $T_{\rm u}=0$ ,  $T_{\rm p}=N_{\rm U}T_{\rm s}$ , and  $T_{\rm f}=0$ . The other baseline scheme is the conventional communication scheme relying on DL channel estimation with the training overhead of  $T_{\rm p} = N_{\rm B} M_{\rm B} T_{\rm s}$ . In this scheme, the perfect knowledge of LOS indicator and angles are assumed to be fed back to each gNB for designing the directional BF, for which the feedback overhead is given by  $T_{\rm f} = \mu_{\rm f} B_{\rm f} T_{\rm s}$  where  $\mu_{\rm f}$ denotes the conversion factor in symbols/bit depending on the employed modulation scheme, and  $B_{\rm f}$  is the feedback amount in bits. The feedback of  $\{\chi_{b,u}: b=1,2,\ldots,N_{\rm B}\}$ and  $\{(\phi_{b,u,0},\theta_{b,u,0}), \forall b: b \in \mathcal{B}_u\}$  from each UE requires  $B_{\mathrm{f}} = N_{\mathrm{U}}N_{\mathrm{B}} + 2Q\sum_{u=1}^{N_{\mathrm{U}}}|\mathcal{B}_u|$  bits in total, where Q is the quantization bits for a real value. We consider Q=8 bits without any quantization error. Meanwhile, the proposed scheme is assumed to use only one symbol period for UL localization, i.e.,  $T_{\rm u} = T_{\rm s}$ . The DL pilot overhead and feedback overhead are given by  $T_p = N_U T_s$  and  $T_f = 0$ , respectively. It is worth noting that the proposed position-assisted communication can increase the achievable rate by reducing the total overhead  $\frac{T_{\rm u}+T_{\rm p}+T_{\rm f}}{T}$  in (34) compared to the conventional scheme.

#### B. Localization Accuracy

In Fig. 4, the root-mean-square error (RMSE) of the proposed SI-based localization using Algorithm 1 is evaluated for different bandwidths in 3GPP scenarios. Specifically, the number of subcarriers  $K_u$  varies in the x-axis for the fixed subcarrier spacing  $\Delta f$ . For a given channel realization, the position estimate is obtained by Algorithm 1 using three different initial points. The localization accuracy is compared to its CRLB provided in (17) and the ideal DP scheme with knowledge of LOS indicators. Fig. 4(a) presents the position error in Indoor-Open office scenario. As the number of subcarriers increases for given  $\Delta f$ , the localization accuracy improves because more observations are available. In particular, the proposed SI-based localization algorithm significantly outperforms the conventional DP scheme with perfect LOS information by exploiting richer information of mmWave propagation environments. It is worth noting that a localization accuracy of less than 0.1 m error can be achieved at  $f_c = 28$  GHz even with 1 MHz bandwidth per UE. Hence,



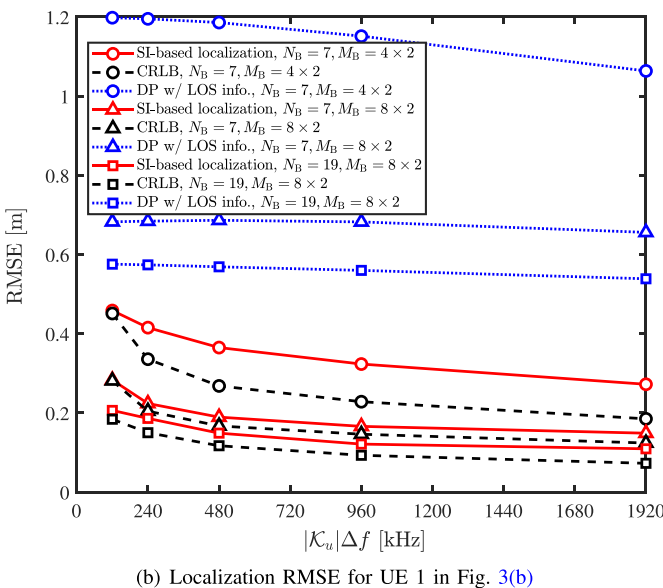


Fig. 4. Position error for different bandwidths:  $N_{\rm s}=300$ .  $|\mathcal{K}_u|$  is the number of subcarriers allocated to the UE. The conventional DP scheme assumes that the LOS indicators are known.

simultaneous localization for multiple UEs is possible with decimeter-level accuracies as a large bandwidth is available in mmWave channels. In addition, it is observed that the MSE gets closer to the theoretical bound as  $M_{\rm B}$  increases. Therefore, the distribution approximation used for designing Algorithm 1 works well particularly for gNBs equipped with a large array. Consequently, our analytic result can be effectively used for providing a design guideline without Monte Carlo simulation. Fig. 4(b) presents the result in the outdoor environment in UMi-Street canyon scenario. Although the MSE is higher than that in the indoor scenario due to the higher pathloss, a decimeter-level localization accuracy can still be achieved depending on the chosen  $M_{\rm B}$  and bandwidth. Moreover, the cooperative localization using  $N_{\rm B}=19~{\rm gNBs}$ leads to a smaller position error, e.g.,  $0.11 \,\mathrm{m}$  at  $|\mathcal{K}_u| = 16$ , compared to the case of  $N_{\rm B}=7$  which has an error of  $0.15\,{\rm m}$ 

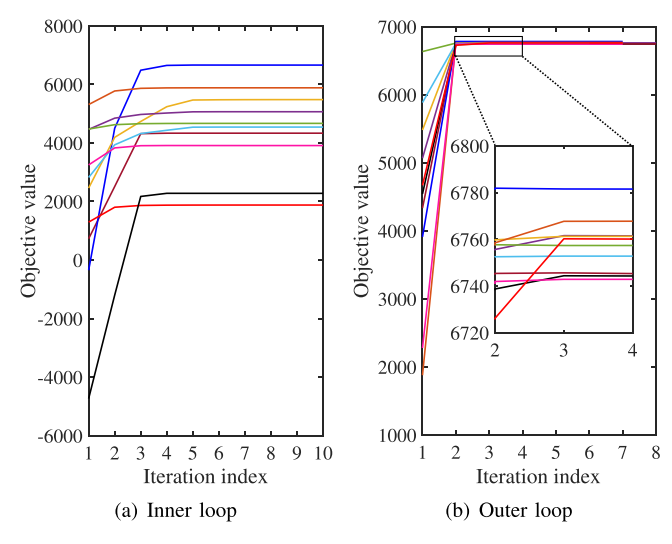


Fig. 5. Convergence behaviors of the inner loop and outer loop in Algorithm 1 for UE 1. The sequences of the objective values are plotted for different random channel realizations and initializations in UMi-Street canyon scenario.  $N_{\rm B}=7,\ M_{\rm B}=4\times2,$  and K=4.

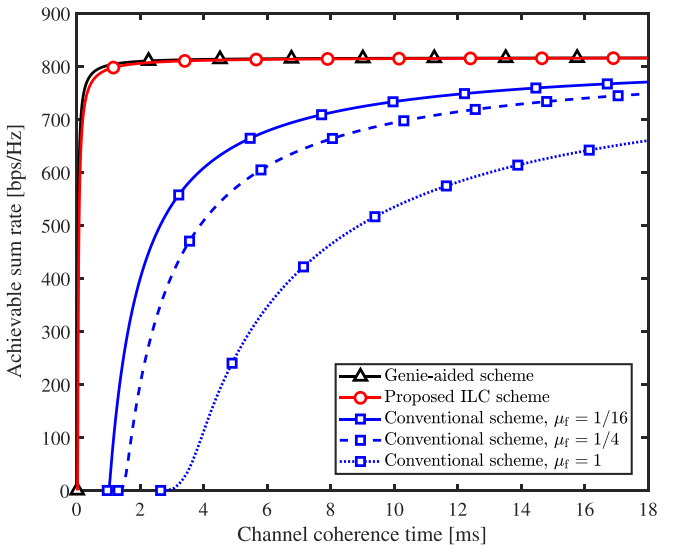
at  $|\mathcal{K}_u| = 16$ . This gain comes from the macrodiversity, which provides an increased likelihood of LOS existence as well as more signal observations. Although cooperation with a large  $N_{\rm B}$  may require a high computational complexity and a high information exchange overhead, one can choose only a subset of gNBs having high received signal strength to efficiently estimate the position with a reduced complexity.

In Fig. 5, the convergence behaviors of the proposed localization algorithm are presented for different random channel realizations and initializations. Fig. 5(a) shows the sequences of the objective values along with the inner iteration at the first outer iteration. The inner loop converges within fewer than ten iterations in most cases. It was observed that the convergence speed of the inner loop is even faster at the next outer iteration. Fig. 5(b) shows the sequences of the objective values along with the outer loop iteration. It can be seen that the algorithm converges within only a few iterations as the second derivatives are used to find the update direction in the algorithm.

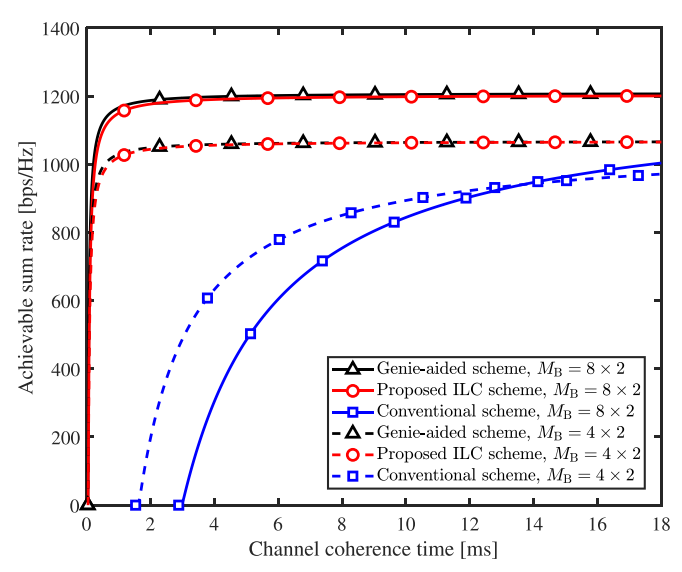
# C. Achievable Sum Rate

In Fig. 6, the average achievable sum rate of the UEs is presented for different channel coherence times using random channel realizations for given 3GPP scenarios. In both Fig. 6(a) and Fig. 6(b), the proposed ILC method outperforms the conventional communication scheme by reducing the pilot and feedback overhead as calculated in the last paragraph of Sec. VI-A. It is remarkable that the proposed scheme is beneficial particularly in short  $T_{\rm c}$  regime, which means that position-assisted communication can play a key role in rapidly changing environments with mobility. For example, in mobile networks for pedestrians with the speed of  $v=4\,{\rm km/h}$  or CAVs with  $v=30\,{\rm km/h}$ ,  $T_{\rm c}$  is given by  $T_{\rm c}=4\,{\rm ms}$  or  $T_{\rm c}=0.54\,{\rm ms}$ , respectively, at  $f_{\rm c}=28\,{\rm GHz}$ , which is shorter than that in static networks or in sub-6 GHz channels.

 $^4T_{\rm c}$  is calculated as  $T_{\rm c}=0.423/f_{\rm D}$  with the maximum Doppler shift  $f_{\rm D}=\frac{v}{c}f_{\rm c}$ , where v is the vehicle speed, and c is the speed of light.



(a) Indoor-Open office:  $N_{\rm U}=2, |\mathcal{K}_u|=8, \forall u, M_{\rm B}=4\times 2$ 



(b) UMi-Street canyon:  $N_{\rm U} = 4$ ,  $|\mathcal{K}_u| = 4$ ,  $\forall u, N_{\rm B} = 19$ ,  $\mu_{\rm f} = 1/16$ 

Fig. 6. Achievable sum rate for different channel coherence times:  $M_{\rm U}=2\times2,~K=16.$  The low-overhead feature of the proposed ILC method becomes more beneficial as  $T_{\rm c}$  decreases with higher mobility or higher  $f_{\rm c}$ .

Moreover, the proposed ILC method approaches the genie-aided scheme with the perfect knowledge of positions and LOS indicators. This is possible because the SI-based localization algorithm provides high accuracy using only one symbol period of localization phase. Fig. 6(b) shows that a larger sum rate is achievable for the proposed scheme using a larger  $M_{\rm B}$ , while the conventional communication scheme may suffer from increased training overhead particularly in short  $T_{\rm c}$  regime.

#### VII. CONCLUSION

This paper developed a cooperative ILC method for mmWave MIMO-OFDM networks. First, an efficient ILC frame structure was proposed for position-assisted communications. Next, the relationship between the received signals and the positions was characterized, which was then used to determine the theoretical limits of mmWave localization. Such analysis also enabled to design an SI-based localization algorithm. The results in 3GPP network scenarios quantify the performance gain of the proposed SI-based localization algorithm with respect to existing techniques, In particular, SI-based localization can achieve decimeter-level accuracy using only a short reference signal even in harsh mmWave environments. Therefore, the proposed ILC method achieves a higher communication rate with a reduced overhead compared to existing techniques, while the position error approaches the theoretical limit. The low overhead of the proposed method is particularly beneficial in scenarios with high mobility. The findings in this paper serve as guidelines to design efficient ILC for mmWave networks with improved localization accuracy and enhanced communication rate in beyond 5G applications.

# APPENDIX A A Proof of Lemma 1

We show that the random vector  $\bar{\mathbf{y}}_{b,u}[K]$  for given  $\mathcal{S}_{b,u}$  and  $p_u$  follows the multivariate Gaussian distribution. From (7),  $\bar{\mathbf{y}}_{b,u}[k]$  for given  $\mathcal{S}_{b,u}=\{\chi_{b,u},\tau_{b,u,l},\phi_{b,u,l},\theta_{b,u,l},\forall l=1,2,\ldots,L-1\}$  can be expressed as

$$\bar{\mathbf{y}}_{b,u}[k] = \left[ \mathbf{B}_{b,u}[k], \mathbf{I}_{kM_{\mathrm{B}}} \right] \begin{bmatrix} \mathbf{\alpha}_{b,u} \\ \bar{\mathbf{n}}_{b,u}[k] \end{bmatrix} + \bar{\boldsymbol{\mu}}_{b,u}^{(\chi_{b,u})}[k]$$
(35)

where

$$\begin{split} \boldsymbol{B}_{b,u}[k] &\triangleq \begin{bmatrix} \boldsymbol{b}_{b,u,1}[k] & \boldsymbol{b}_{b,u,2}[k] & \cdots & \boldsymbol{b}_{b,u,L-1}[k] \\ \boldsymbol{b}_{b,u,1}[k-1] & \boldsymbol{b}_{b,u,2}[k-1] & \cdots & \boldsymbol{b}_{b,u,L-1}[k-1] \\ \vdots & \vdots & \ddots & \vdots \\ \boldsymbol{b}_{b,u,1}[1] & \boldsymbol{b}_{b,u,2}[1] & \cdots & \boldsymbol{b}_{b,u,L-1}[1] \end{bmatrix} \\ \boldsymbol{b}_{b,u,l}[k] &\triangleq \sqrt{\varrho_{b,u,l}} M_{\mathrm{B}} P_{\mathrm{t}} \tilde{\boldsymbol{h}}_{b,u}^{(\mathrm{N})} e^{-j2\pi k \Delta f \tau_{b,u,l}} \boldsymbol{a}_{\mathrm{B}} (\phi_{b,u,l}, \theta_{b,u,l}) \\ \boldsymbol{\alpha}_{b,u} &\triangleq \begin{bmatrix} \boldsymbol{\alpha}_{b,u,1}, \boldsymbol{\alpha}_{b,u,2}, \cdots, \boldsymbol{\alpha}_{b,u,L-1} \end{bmatrix}^{\mathrm{T}} \\ \bar{\boldsymbol{n}}_{b,u}[k] &\triangleq \begin{bmatrix} (\boldsymbol{n}_{b,u}[k])^{\mathrm{T}}, (\boldsymbol{n}_{b,u}[k-1])^{\mathrm{T}}, \cdots, (\boldsymbol{n}_{b,u}[1])^{\mathrm{T}} \end{bmatrix}^{\mathrm{T}}. \end{split}$$

Since (35) can be seen as an affine transformation of independent Gaussian RVs in  $\alpha_{b,u}$  and  $\bar{\mathbf{n}}_{b,u}$ , the random vector  $\bar{\mathbf{y}}_{b,u}[k]$  for given  $\mathsf{S}_{b,u}=\mathcal{S}_{b,u}$  follows the multivariate Gaussian distribution. The mean vector and covariance matrix given in (11) can be easily calculated from the following definitions

$$\begin{split} \bar{\boldsymbol{\mu}}_{b,u}^{(\chi_{b,u})}[k] &\triangleq \mathbb{E}\left\{\bar{\mathbf{y}}_{b,u}[k] | \mathsf{S}_{b,u} = \mathcal{S}_{b,u}\right\} \\ \bar{\boldsymbol{\Sigma}}_{b,u}[k] &\triangleq \mathbb{E}\left\{\left(\bar{\mathbf{y}}_{b,u}[k] - \bar{\boldsymbol{\mu}}_{b,u}^{(\chi_{b,u})}[k]\right) \left(\bar{\mathbf{y}}_{b,u}[k] - \bar{\boldsymbol{\mu}}_{b,u}^{(\chi_{b,u})}[k]\right)^{\dagger} \\ & \left|\mathsf{S}_{b,u} = \mathcal{S}_{b,u}\right\}. \end{split}$$

# APPENDIX B A Proof of Proposition 1

From Lemma 1, we have

$$f_{\bar{\mathbf{y}}_{b,u}[k]|S_{b,u}}(\bar{\mathbf{y}}_{b,u}[k]|S_{b,u}; \boldsymbol{p}_{u})$$

$$= \varphi(\bar{\mathbf{y}}_{b,u}[k]; \bar{\boldsymbol{\mu}}_{b,u}^{(\chi_{b,u})}[k], \bar{\boldsymbol{\Sigma}}_{b,u}[k]). \quad (36)$$

The mean vector  $ar{\pmb{\mu}}_{b,u}^{(\chi_{b,u})}[k]$  and the covariance matrix  $ar{\pmb{\Sigma}}_{b,u}[k]$ 

$$\begin{split} & \bar{\boldsymbol{\mu}}_{b,u}^{(\chi_{b,u})}[k] = & \Big[ \big( \boldsymbol{\mu}_{b,u}^{(\chi_{b,u})}[k] \big)_{,}^{\mathbf{T}} \, \big( \boldsymbol{\mu}_{b,u}^{(\chi_{b,u})}[k-1] \big)_{,}^{\mathbf{T}} \cdots, \big( \boldsymbol{\mu}_{b,u}^{(\chi_{b,u})}[1] \big)_{,}^{\mathbf{T}} \Big]_{,}^{\mathbf{T}} \\ & \bar{\boldsymbol{\Sigma}}_{b,u}[k] = \begin{bmatrix} \bar{\boldsymbol{\Sigma}}_{b,u}^{(1,1)}[k] & \bar{\boldsymbol{\Sigma}}_{b,u}^{(1,2)}[k] \\ \bar{\boldsymbol{\Sigma}}_{b,u}^{(2,2)}[k] & \bar{\boldsymbol{\Sigma}}_{b,u}^{(2,2)}[k] \end{bmatrix} \end{split}$$

$$\boldsymbol{\mu}_{b,u}^{(\chi_{b,u})}[k] = \chi_{b,u} \sqrt{M_{\rm B} P_{\rm t} \tilde{h}_{b,u}^{(\rm L)}} e^{-\imath 2\pi k \Delta f \tau_{b,u,0}} \boldsymbol{a}_{\rm B}(\phi_{b,u,0}, \theta_{b,u,0})$$
(37a)

$$\bar{\Sigma}_{b,u}^{(1,1)}[k] = \xi_{b,u} \sum_{l=1}^{L-1} \varrho_{b,u,l} \mathbf{A}_{b,u,l} + P_{\mathbf{n}} \mathbf{I}_{M_{\mathbf{B}}}$$
(37b)

$$\bar{\mathbf{\Sigma}}_{b,u}^{(1,2)}[k] = \xi_{b,u} \sum_{l=1}^{L-1} \varrho_{b,u,l} \left[ \rho_{b,u,l}^{(-1)}, \rho_{b,u,l}^{(-2)}, \cdots, \rho_{b,u,l}^{(-k+1)} \right] \otimes \mathbf{A}_{b,u,l}$$
(37c)

$$\bar{\boldsymbol{\Sigma}}_{b,u}^{(2,1)}[k] = \xi_{b,u} \sum_{l=1}^{L-1} \varrho_{b,u,l} \left[ \rho_{b,u,l}^{(1)}, \rho_{b,u,l}^{(2)}, \cdots, \rho_{b,u,l}^{(k-1)} \right]^{\mathrm{T}} \otimes \boldsymbol{A}_{b,u,l}$$

$$\bar{\Sigma}_{b,u}^{(2,2)}[k] = \bar{\Sigma}_{b,u}[k-1] \tag{37e}$$

with  $\xi_{b,u} \triangleq M_{\rm B} P_{\rm t} \tilde{h}_{b,u}^{({\rm N})}$ . Note that  $\bar{\mathcal{D}}_{b,u}^{(1,1)}[k]$  is constant for all k. Using (37), the PDF in (36) can be factorized as

$$f_{\bar{\mathbf{y}}_{b,u}[K]|S_{b,u}}(\bar{\mathbf{y}}_{b,u}[K]|S_{b,u}; \mathbf{p}_{u})$$

$$= f_{\mathbf{y}_{b,u}[1]|S_{b,u}}(\mathbf{y}_{b,u}[1]|S_{b,u}; \mathbf{p}_{u})$$

$$\times \prod_{k=2}^{K} f_{\mathbf{y}_{b,u}[k]|\bar{\mathbf{y}}_{b,u}[k-1],S_{b,u}}(\mathbf{y}_{b,u}[k]|\bar{\mathbf{y}}_{b,u}[k-1],S_{b,u}; \mathbf{p}_{u})$$

$$= \prod_{k=1}^{K} \varphi(\mathbf{y}_{b,u}[k]; \hat{\boldsymbol{\mu}}_{b,u}^{(\chi_{b,u})}[k], \hat{\boldsymbol{\Sigma}}_{b,u}[k])$$
(38)

where the mean vector and covariance matrix of  $\mathbf{y}_{b,u}[k]$  for given  $\bar{y}_{b,u}[k-1]$  and  $S_{b,u}$  are given as [70]

$$\hat{\boldsymbol{\mu}}_{b,u}^{(\chi_{b,u})}[k] = \boldsymbol{\mu}_{b,u}^{(\chi_{b,u})}[k] + \bar{\boldsymbol{\Sigma}}_{b,u}^{(1,2)}[k] \left(\bar{\boldsymbol{\Sigma}}_{b,u}^{(2,2)}[k]\right)^{-1} \times \left(\bar{\boldsymbol{y}}_{b,u}[k-1] - \bar{\boldsymbol{\mu}}_{b,u}^{(\chi_{b,u})}[k-1]\right)$$
(39)

$$\hat{\Sigma}_{b,u}[k] = \bar{\Sigma}_{b,u}^{(1,1)}[k] - \bar{\Sigma}_{b,u}^{(1,2)}[k] \left(\bar{\Sigma}_{b,u}^{(2,2)}[k]\right)^{-1} \bar{\Sigma}_{b,u}^{(2,1)}[k]. \tag{40}$$

#### APPENDIX C

#### Transformation Matrix in (19)

In (19), the transformation matrix  $\frac{\partial \boldsymbol{\eta}_{b,u}^{\mathrm{T}}}{\partial \boldsymbol{p}_{u}} \in \mathbb{R}^{3\times3}$  is derived

$$\frac{\partial \phi_{b,u,0}}{\partial \boldsymbol{p}_{u}} = \frac{\mathring{p}_{b,u,x} \boldsymbol{k}_{2} - \mathring{p}_{b,u,y} \boldsymbol{k}_{1}}{\mathring{p}_{r}^{2} + \mathring{p}_{r}^{2}}$$
(41a)

$$\frac{\partial \phi_{b,u,0}}{\partial \boldsymbol{p}_{u}} = \frac{\mathring{p}_{b,u,x} \boldsymbol{k}_{2} - \mathring{p}_{b,u,y} \boldsymbol{k}_{1}}{\mathring{p}_{b,u,x}^{2} + \mathring{p}_{b,u,y}^{2}} \tag{41a}$$

$$\frac{\partial \theta_{b,u,0}}{\partial \boldsymbol{p}_{u}} = \frac{-1}{\sqrt{\mathring{p}_{b,u,x}^{2} + \mathring{p}_{b,u,y}^{2}}} \left(\frac{\mathring{p}_{b,u,z}}{\|\mathring{\boldsymbol{p}}_{b,u}\|^{2}} (\boldsymbol{p}_{u} - \boldsymbol{q}_{b}) - \boldsymbol{k}_{3}\right) \tag{41b}$$

$$\frac{\partial \tau_{b,u,0}}{\partial \boldsymbol{p}_u} = \frac{1}{c} \frac{\boldsymbol{p}_u - \boldsymbol{q}_b}{\|\boldsymbol{p}_u - \boldsymbol{q}_b\|}$$
(41c)

where  $\mathring{p}_{b,u}$  is given in (4), and  $k_i$  is the *i*th column vector of  $K(\phi,\theta)$  in (5).

# APPENDIX D A PROOF OF PROPOSITION 2

For simplicity, we omit the superscript (n) in  $\mathcal{S}_{b,u}^{(n)}$ . From the relation between the joint and conditional FIMs of multiple observations [71], the FIM in (20), which accounts for all subcarriers included in  $\bar{\mathbf{y}}_{b,u}[K]$  for given  $\mathcal{S}_{b,u}$ , can be expressed by the sum of conditional FIMs of each subcarrier as follows,

$$\boldsymbol{J}^{(b)}(\boldsymbol{\eta}_{b,u}\big|\mathcal{S}_{b,u}) = \sum_{k=1}^{K} \boldsymbol{J}_{k|k-1}^{(b)}(\boldsymbol{\eta}_{b,u}\big|\mathcal{S}_{b,u})$$
(42)

where  $J_{k|k-1}^{(b)}(\eta_{b,u}|\mathcal{S}_{b,u})$  denotes the conditional FIM of  $\mathbf{y}_{b,u}[k]$  for given  $\bar{\mathbf{y}}_{b,u}[k-1]$  and  $\mathcal{S}_{b,u}$ . In particular, this conditional FIM is defined by

$$J_{k|k-1}^{(b)}(\boldsymbol{\eta}_{b,u}|\mathcal{S}_{b,u})$$

$$\triangleq \mathbb{E}\left\{\frac{\partial \ln f(\mathbf{y}_{b,u}[k]|\bar{\mathbf{y}}_{b,u}[k-1],\mathcal{S}_{b,u};\boldsymbol{\eta}_{b,u})}{\partial \boldsymbol{\eta}_{b,u}} \times \frac{\partial \ln f(\mathbf{y}_{b,u}[k]|\bar{\mathbf{y}}_{b,u}[k-1],\mathcal{S}_{b,u};\boldsymbol{\eta}_{b,u})}{\partial \boldsymbol{\eta}_{b,u}^{\mathrm{T}}} |\mathcal{S}_{b,u}| \mathcal{S}_{b,u} \right\}$$
(43)

with  $f(\mathbf{y}_{b,u}[1]|\bar{\mathbf{y}}_{b,u}[0], \mathcal{S}_{b,u}; \eta_{b,u}) \triangleq f(\mathbf{y}_{b,u}[1]|\mathcal{S}_{b,u}; \eta_{b,u})$ . In (43), the expectation is taken over both  $\mathbf{y}_{b,u}[k]$  and  $\bar{\mathbf{y}}_{b,u}[k-1]$ , which can be calculated by the law of iterated expectations  $\mathbb{E}_{\mathbf{y}_{b,u}[k],\bar{\mathbf{y}}_{b,u}[k-1]}\{\cdot|\mathcal{S}_{b,u}\} = \mathbb{E}_{\bar{\mathbf{y}}_{b,u}[k-1]}\{\mathbb{E}_{\mathbf{y}_{b,u}[k]}\{\cdot|\bar{\mathbf{y}}_{b,u}[k-1],\mathcal{S}_{b,u}\},\mathcal{S}_{b,u}\}$ . Since the conditional PDF of  $\mathbf{y}_{b,u}[k]$  for given  $\bar{\mathbf{y}}_{b,u}[k-1]$  and  $\mathcal{S}_{b,u}$  follows the Gaussian distribution as in (13), the inner expectation can be calculated using the result in [72, Appendix 15C]. Then the *i*th row and the *j*th column of the conditional FIM in (43) can be expressed as

$$\begin{split} & \left[ \boldsymbol{J}_{k|k-1}^{(b)}(\boldsymbol{\eta}_{b,u}|\mathcal{S}_{b,u}) \right]_{i,j} \\ &= \operatorname{tr} \Big( \hat{\boldsymbol{\Sigma}}_{b,u}^{-1}[k] \frac{\partial \hat{\boldsymbol{\Sigma}}_{b,u}[k]}{\partial [\boldsymbol{\eta}_{b,u}]_i} \ \hat{\boldsymbol{\Sigma}}_{b,u}^{-1}[k] \frac{\partial \hat{\boldsymbol{\Sigma}}_{b,u}[k]}{\partial [\boldsymbol{\eta}_{b,u}]_j} \Big) \\ &+ 2 \Re \Big\{ \underbrace{\mathbb{E}_{\bar{\boldsymbol{y}}_{b,u}[k-1]} \Big\{ \frac{\partial \left(\hat{\boldsymbol{\mu}}_{b,u}^{(\chi_{b,u})}[k]\right)^{\dagger}}{\partial [\boldsymbol{\eta}_{b,u}]_i} \hat{\boldsymbol{\Sigma}}_{b,u}^{-1}[k] \frac{\partial \hat{\boldsymbol{\mu}}_{b,u}^{(\chi_{b,u})}[k]}{\partial [\boldsymbol{\eta}_{b,u}]_j} \Big| \mathcal{S}_{b,u} \Big\} \Big\} \\ &\triangleq \nu_{i,j} \end{split}$$

where  $\hat{\mathbf{\mu}}_{b,u}^{(\chi_{b,u})}[k]$  and  $\hat{\mathbf{\Sigma}}_{b,u}[k]$  are defined in (14) and (15).

The expression in (44) can be calculated in a closed-form for each variable in  $\eta_{b,u} = [\phi_{b,u,0}, \theta_{b,u,0}, \tau_{b,u,0}]^{\mathrm{T}}$ . Here, the following short notations are used for brevity

$$\bar{\Sigma}'_{b,u}[k] \triangleq \begin{cases} \mathbf{0} & \text{if } k = 1\\ \bar{\Sigma}_{b,u}^{(1,2)}[k] \left(\bar{\Sigma}_{b,u}^{(2,2)}[k]\right)^{-1} & \text{if } k > 1 \end{cases}$$
(45)

$$\bar{\rho}[k] \triangleq \left[ \rho_{b,u,0}^{(-k)}, \rho_{b,u,0}^{(-k+1)}, \dots, \rho_{b,u,0}^{(-1)} \right]^{\mathrm{T}}.$$
 (46)

Using (45), the partial derivative  $\frac{\partial \hat{\Sigma}_{b,u}[k]}{\partial [\eta_{b,u}]_i}$  in tr(·) of (44) can be derived as

$$\frac{\partial \hat{\mathbf{\Sigma}}_{b,u}[k]}{\partial [\boldsymbol{\eta}_{b,u}]_{i}} = \begin{cases}
\mathbf{0} & \text{if } i = 1, 2 \\
\frac{\partial \bar{\mathbf{\Sigma}}_{b,u}^{(1,1)}[k]}{\partial \tau_{b,u,0}} + \frac{\beta_{N}}{\tau_{b,u,0}} \bar{\mathbf{\Sigma}}'_{b,u}[k] \bar{\mathbf{\Sigma}}_{b,u}^{(2,1)}[k] & \text{if } i = 3
\end{cases}$$

where  $\frac{\partial \bar{\mathcal{E}}_{b,u}^{(1,1)}[k]}{\partial \tau_{b,u,0}} = -\frac{\beta_{\mathrm{N}}}{\tau_{b,u,0}} M_{\mathrm{B}} P_{\mathrm{t}} \tilde{h}_{b,u}^{(\mathrm{N})} \sum_{l=1}^{L-1} \varrho_{b,u,l} A_{b,u,l}$ . Note that (47) becomes zero when i=1,2 because  $\hat{\mathcal{L}}_{b,u}[k]$  is independent of  $\phi_{b,u,0}$  and  $\theta_{b,u,0}$ . Meanwhile, the term  $\nu_{i,j}$  in (44) is derived as follows

$$\nu_{i,j} = \chi_{b,u} M_{\rm B} P_{\rm t} \tilde{h}_{b,u}^{(\rm L)} \dot{\boldsymbol{\mu}}_{b,u,i}^{\dagger}[k] \hat{\boldsymbol{\mathcal{L}}}_{b,u}^{-1}[k] \dot{\boldsymbol{\mu}}_{b,u,j}[k]$$
(48)

where  $\dot{\mu}_{b.u.i}^{\dagger}[k]$  is defined using (45) and (46) as

$$\dot{\boldsymbol{\mu}}_{b,u,1}[k] \triangleq e^{-\imath 2\pi k \Delta f \tau_{b,u,0}} \dot{\boldsymbol{a}}_{\mathrm{B},\phi} - \bar{\boldsymbol{\Sigma}}'_{b,u}[k] \left( \bar{\boldsymbol{\rho}}[k-1] \otimes \dot{\boldsymbol{a}}_{\mathrm{B},\phi} \right)$$
(49a)

$$\dot{\boldsymbol{\mu}}_{b,u,2}[k] \triangleq e^{-\imath 2\pi k \Delta f \tau_{b,u,0}} \dot{\boldsymbol{a}}_{\mathrm{B},\theta} - \bar{\boldsymbol{\Sigma}}'_{b,u}[k] \left( \bar{\boldsymbol{\rho}}[k-1] \otimes \dot{\boldsymbol{a}}_{\mathrm{B},\theta} \right) \tag{49b}$$

$$\dot{\boldsymbol{\mu}}_{b,u,3}[k] \triangleq \left(\frac{-\beta_{\mathrm{L}}}{2\tau_{b,u,0}} - i2\pi k\Delta f\right) e^{-i2\pi k\Delta f \tau_{b,u,0}} \boldsymbol{a}_{\mathrm{B}}(\phi_{b,u,0},\theta_{b,u,0})$$

$$-\frac{\beta_{\mathrm{L}}}{2\tau_{b,u,0}} \bar{\boldsymbol{\Sigma}}'_{b,u}[k] \left(\bar{\boldsymbol{\rho}}[k-1] \otimes \boldsymbol{a}_{\mathrm{B}}(\phi_{b,u,0},\theta_{b,u,0})\right)$$

$$+\bar{\boldsymbol{\Sigma}}'_{b,u}[k] \frac{\partial \left(\bar{\boldsymbol{\rho}}[k-1] \otimes \boldsymbol{a}_{\mathrm{B}}(\phi_{b,u,0},\theta_{b,u,0})\right)}{\partial \tau_{b,u,0}} \tag{49c}$$

with

$$\dot{\boldsymbol{a}}_{\mathrm{B},\phi} \triangleq -i \frac{\partial \boldsymbol{G}_{\mathrm{B}}^{\mathrm{T}} \boldsymbol{k}(\phi_{b,u,0}, \theta_{b,u,0})}{\partial \phi_{b,u,0}} \odot \boldsymbol{a}_{\mathrm{B}}(\phi_{b,u,0}, \theta_{b,u,0})$$
 (50a)

$$\dot{\boldsymbol{a}}_{\mathrm{B},\theta} \triangleq -i \frac{\partial \boldsymbol{G}_{\mathrm{B}}^{\mathrm{T}} \boldsymbol{k} (\phi_{b,u,0}, \theta_{b,u,0})}{\partial \theta_{b,u,0}} \odot \boldsymbol{a}_{\mathrm{B}} (\phi_{b,u,0}, \theta_{b,u,0}) \quad (50b)$$

$$G_{\mathrm{B}} \triangleq [g_{\mathrm{B},1}, g_{\mathrm{B},2}, \dots, g_{\mathrm{B},M_{\mathrm{B}}}] \in \mathbb{R}^{3 \times M_{\mathrm{B}}}.$$
 (50c)

In (50c),  $g_{B,m}$  is the relative position vector of the mth antenna element with  $g_{B,1} = 0_{3\times 1}$ .

#### APPENDIX E

# THE GRADIENT AND HESSIAN MATRIX IN ALGORITHM 1

In this section, the elements of the gradient and Hessian matrix of  $\ell_u(p_u; p_u^{(t-1)})$  in (26) are derived, which are used in Algorithm 1.

## A. Gradient $\nabla \ell_u$

The gradient  $\nabla \ell_u$  is defined by  $\nabla \ell_u = \left[\frac{\partial \ell_u}{\partial p_x^u}, \frac{\partial \ell_u}{\partial p_y^u}, \frac{\partial \ell_u}{\partial p_z^u}\right]^T$ . Using the chain rule for derivative of multi-variable functions,  $\nabla \ell_u$  is expressed as

$$\nabla \ell_{u} = \begin{bmatrix} \sum_{b=1}^{N_{\rm B}} \left( \frac{\partial \ell_{u}}{\partial \phi_{b,u,0}} \frac{\partial \phi_{b,u,0}}{\partial p_{u}^{x}} + \frac{\partial \ell_{u}}{\partial \theta_{b,u,0}} \frac{\partial \theta_{b,u,0}}{\partial p_{u}^{x}} + \frac{\partial \ell_{u}}{\partial r_{b,u}} \frac{\partial r_{b,u}}{\partial p_{u}^{x}} \right) \\ \sum_{b=1}^{N_{\rm B}} \left( \frac{\partial \ell_{u}}{\partial \phi_{b,u,0}} \frac{\partial \phi_{b,u,0}}{\partial p_{u}^{y}} + \frac{\partial \ell_{u}}{\partial \theta_{b,u,0}} \frac{\partial \theta_{b,u,0}}{\partial p_{u}^{y}} + \frac{\partial \ell_{u}}{\partial r_{b,u}} \frac{\partial r_{b,u}}{\partial p_{u}^{y}} \right) \\ \sum_{b=1}^{N_{\rm B}} \left( \frac{\partial \ell_{u}}{\partial \phi_{b,u,0}} \frac{\partial \phi_{b,u,0}}{\partial p_{u}^{z}} + \frac{\partial \ell_{u}}{\partial \theta_{b,u,0}} \frac{\partial \theta_{b,u,0}}{\partial p_{u}^{z}} + \frac{\partial \ell_{u}}{\partial r_{b,u}} \frac{\partial r_{b,u}}{\partial p_{u}^{z}} \right) \end{bmatrix}.$$

$$(51)$$

The partial derivatives  $\frac{\partial \ell_u}{\partial \phi_{b,u,0}}$ ,  $\frac{\partial \ell_u}{\partial \theta_{b,u,0}}$ , and  $\frac{\partial \ell_u}{\partial r_{b,u}}$  in (51) are derived first. Then the remaining terms will be given.

Define the following constants for given  $p_u^{(t-1)}$ 

$$\xi_{b,u}^{(L)} \triangleq f_{\mathbf{X}_{b,u}|\bar{\mathbf{y}}_{b,u}[K]} \left( 1 \middle| \bar{\mathbf{y}}_{b,u}[K]; \boldsymbol{p}_{u}^{(t-1)} \right)$$
 (52a)

$$\xi_{b,u}^{(\mathrm{N})} \triangleq f_{\mathbf{X}_{b,u}|\bar{\mathbf{y}}_{b,u}[K]}(0|\bar{\boldsymbol{y}}_{b,u}[K];\boldsymbol{p}_{u}^{(t-1)})$$
 (52b)

which are independent of  $p_u$  and are calculated from (25). Using (26) and (52), the partial derivatives  $\frac{\partial \ell_u}{\partial \phi_{b,u,0}}$ ,  $\frac{\partial \ell_u}{\partial \theta_{b,u,0}}$ , and  $\frac{\partial \ell_u}{\partial r_{b,u}}$  in (51) can be obtained as

$$\frac{\partial \ell_{u}}{\partial \phi_{b,u,0}} = \xi_{b,u}^{(L)} \sum_{k=1}^{K} \frac{\partial}{\partial \phi_{b,u,0}} \ln \varphi \left( \mathbf{y}_{b,u}[k]; \tilde{\boldsymbol{\mu}}_{b,u}^{(1)}[k], \tilde{\boldsymbol{\Sigma}}_{b,u}[k] \right)$$
(53a)

$$\frac{\partial \ell_{u}}{\partial \theta_{b,u,0}} = \xi_{b,u}^{(L)} \sum_{k=1}^{K} \frac{\partial}{\partial \theta_{b,u,0}} \ln \varphi \left( \mathbf{y}_{b,u}[k]; \tilde{\boldsymbol{\mu}}_{b,u}^{(1)}[k], \tilde{\boldsymbol{\Sigma}}_{b,u}[k] \right)$$
(53b)

$$\frac{\partial \ell_{u}}{\partial r_{b,u}} = \xi_{b,u}^{(L)} \frac{\partial}{\partial r_{b,u}} \ln p_{L}(r_{b,u}) + \xi_{b,u}^{(N)} \frac{\partial}{\partial r_{b,u}} \ln \left(1 - p_{L}(r_{b,u})\right) 
+ \xi_{b,u}^{(L)} \sum_{k=1}^{K} \frac{\partial}{\partial r_{b,u}} \ln \varphi \left(\boldsymbol{y}_{b,u}[k]; \tilde{\boldsymbol{\mu}}_{b,u}^{(1)}[k], \tilde{\boldsymbol{\Sigma}}_{b,u}[k]\right) 
+ \xi_{b,u}^{(N)} \sum_{k=1}^{K} \frac{\partial}{\partial r_{b,u}} \ln \varphi \left(\boldsymbol{y}_{b,u}[k]; \tilde{\boldsymbol{\mu}}_{b,u}^{(0)}[k], \tilde{\boldsymbol{\Sigma}}_{b,u}[k]\right)$$
(53c)

where  $\tilde{\boldsymbol{\mu}}_{b,u}^{(0)}[k]$  and  $\tilde{\boldsymbol{\Sigma}}_{b,u}[k]$  are functions of  $r_{b,u}$ , while  $\tilde{\boldsymbol{\mu}}_{b,u}^{(1)}[k]$  is a function of  $\phi_{b,u,0}$ ,  $\theta_{b,u,0}$ , and  $r_{b,u}$ . The partial derivatives of  $\ln \varphi(\boldsymbol{y}_{b,u}[k]; \tilde{\boldsymbol{\mu}}_{b,u}^{(\lambda_{b,u})}[k], \tilde{\boldsymbol{\Sigma}}_{b,u}[k])$  with respect to  $\boldsymbol{\eta}_{b,u}' \triangleq [\phi_{b,u,0}, \theta_{b,u,0}, r_{b,u}]^{\mathrm{T}}$  is given by [72]

$$\frac{\partial}{\partial [\boldsymbol{\eta}_{b,u}']_{i}} \ln \varphi \left( \boldsymbol{y}_{b,u}[k]; \tilde{\boldsymbol{\mu}}_{b,u}^{(\chi_{b,u})}[k], \tilde{\boldsymbol{\Sigma}}_{b,u}[k] \right) 
= -\text{tr} \left( \tilde{\boldsymbol{\Sigma}}_{b,u}^{-1}[k] \frac{\partial \tilde{\boldsymbol{\Sigma}}_{b,u}[k]}{\partial [\boldsymbol{\eta}_{b,u}']_{i}} \right) 
+ \left( \tilde{\boldsymbol{z}}_{b,u}^{(\chi_{b,u})}[k] \right)^{\dagger} \tilde{\boldsymbol{\Sigma}}_{b,u}^{-1}[k] \frac{\partial \tilde{\boldsymbol{\Sigma}}_{b,u}[k]}{\partial [\boldsymbol{\eta}_{b,u}']_{i}} \tilde{\boldsymbol{\Sigma}}_{b,u}^{-1}[k] \tilde{\boldsymbol{z}}_{b,u}^{(\chi_{b,u})}[k] 
+ 2\Re \left\{ \left( \tilde{\boldsymbol{z}}_{b,u}^{(\chi_{b,u})}[k] \right)^{\dagger} \tilde{\boldsymbol{\Sigma}}_{b,u}^{-1}[k] \frac{\partial \tilde{\boldsymbol{\mu}}_{b,u}^{(\chi_{b,u})}[k]}{\partial [\boldsymbol{\eta}_{b,u}']_{i}} \right\}$$
(54)

with  $\tilde{\boldsymbol{z}}_{b,u}^{(\chi_{b,u})}[k] \triangleq \boldsymbol{y}_{b,u}[k] - \tilde{\boldsymbol{\mu}}_{b,u}^{(\chi_{b,u})}[k]$ . In (54), the derivatives of  $\tilde{\boldsymbol{\mu}}_{b,u}^{(\chi_{b,u})}[k]$  and  $\tilde{\boldsymbol{\Sigma}}_{b,u}[k]$  are obtained as

$$\frac{\partial \tilde{\boldsymbol{\mu}}_{b,u}^{(1)}[k]}{\partial [\boldsymbol{\eta}_{b,u}']_{i}} = \frac{\partial \boldsymbol{\mu}_{b,u}^{(1)}[k]}{\partial [\boldsymbol{\eta}_{b,u}']_{i}} - \bar{\boldsymbol{\Sigma}}_{b,u}'[k] \frac{\partial \bar{\boldsymbol{\mu}}_{b,u}^{(1)}[k-1]}{\partial [\boldsymbol{\eta}_{b,u}']_{i}}, \forall i \in \{1,2,3\} 
\frac{\partial \tilde{\boldsymbol{\mu}}_{b,u}^{(0)}[k]}{\partial [\boldsymbol{\eta}_{b,u}']_{i}} = \mathbf{0}, \ \forall i \in \{1,2,3\}$$

$$\frac{\partial \tilde{\boldsymbol{\Sigma}}_{b,u}[k]}{\partial [\boldsymbol{\eta}_{b,u}']_i} = \begin{cases} \boldsymbol{0} & \text{if } i \in \{1,2\} \\ \frac{\beta_{\mathrm{N}}}{r_{b,u}} (P_{\mathrm{n}}\boldsymbol{I} - \tilde{\boldsymbol{\Sigma}}_{b,u}[k]) & \text{if } i = 3 \end{cases}$$

with

$$\begin{split} &\frac{\partial \boldsymbol{\mu}_{b,u}^{(1)}[k]}{\partial [\boldsymbol{\eta}_{b,u}']_{i}} \\ &= \begin{cases} -\imath \frac{\partial \boldsymbol{G}_{\mathrm{B}}^{\mathrm{T}} \boldsymbol{k}(\phi_{b,u,0},\theta_{b,u,0})}{\partial [\boldsymbol{\eta}_{b,u}']_{i}} \odot \boldsymbol{\mu}_{b,u}^{(1)}[k] & \text{if } i \in \{1,2\} \\ -\left(\frac{\beta_{\mathrm{L}}}{2r_{b,u}} + \imath 2\pi k \Delta f \frac{1}{c}\right) \boldsymbol{\mu}_{b,u}^{(1)}[k] & \text{if } i = 3 \end{cases} \end{split}$$

where  $G_{\rm B}$  is defined in (50c). The derivative  $\frac{\partial \bar{\mu}_{b,u}^{(1)}[k-1]}{\partial [\eta_{b,u}']_i}$  can be obtained by concatenating  $\frac{\partial \mu_{b,u}^{(1)}[k']}{\partial [\eta_{b,u}']_i}$  for  $k'=k-1,k-2,\ldots,1$ . The matrix  $\bar{\bar{\Sigma}}_{b,u}'[k]$  is defined in the same way with  $\bar{\Sigma}_{b,u}'[k]$  in (45) as

$$\bar{\bar{\Sigma}}'_{b,u}[k] \triangleq \begin{cases} \mathbf{0} & \text{if } k = 1\\ \bar{\bar{\Sigma}}^{(1,2)}_{b,u}[k] (\bar{\bar{\Sigma}}^{(2,2)}_{b,u}[k])^{-1} & \text{if } k > 1 \end{cases}$$
(55)

where the submatrices  $\bar{\Sigma}_{b,u}^{(1,2)}[k]$  and  $\bar{\Sigma}_{b,u}^{(2,2)}[k]$  are defined in the same way with  $\bar{\Sigma}_{b,u}^{(1,2)}[k]$  and  $\bar{\Sigma}_{b,u}^{(2,2)}[k]$ , respectively, in Sec. III-A. Meanwhile, in (53c),  $\frac{\partial}{\partial r_{b,u}} \ln p_{\rm L}(r_{b,u})$  and  $\frac{\partial}{\partial r_{b,u}} \ln \left(1 - p_{\rm L}(r_{b,u})\right)$  can be derived for given LOS probability models depending on the considered scenario, e.g., Indoor-Open office and UMi-Street canyon in 3GPP.

Next,  $\frac{\partial \phi_{b,u,0}}{\partial \boldsymbol{p}_u}$  and  $\frac{\partial \theta_{b,u,0}}{\partial \boldsymbol{p}_u}$  in (51) can be found in (41a) and (41b), respectively. The derivative  $\frac{\partial r_{b,u}}{\partial \boldsymbol{p}_u}$  is given by

$$\frac{\partial r_{b,u}}{\partial \boldsymbol{p}_{u}} = \frac{1}{r_{b,u}} \left( \boldsymbol{p}_{u} - \boldsymbol{q}_{b} \right). \tag{56}$$

From (53a), (53b), (53c), (41a), (41b), and (56), the elements of  $\nabla \ell_u$  in (51) can be obtained.

# B. Hessian Matrix $\nabla^2 \ell_n$

Using (51), the Hessian matrix can be obtained as

$$\nabla^2 \ell_u = \frac{\partial}{\partial \boldsymbol{p}_u} (\nabla \ell_u)^{\mathrm{T}}.$$
 (57)

We only present the element on the first column and first row of the matrix  $\nabla^2 \ell_u$ , i.e.,  $\frac{\partial^2 \ell_u}{\partial p_u^x \partial p_u^x}$ , for brevity. From the right-hand side of (51), the second derivative of  $\ell_u$  with respect to  $p_u^x$  can be expressed by the chain rule as

$$\frac{\partial^{2} \ell_{u}}{\partial p_{u}^{\mathsf{x}} \partial p_{u}^{\mathsf{x}}} = \sum_{b=1}^{N_{\mathsf{B}}} \frac{\partial^{2} \ell_{u}}{\partial p_{u}^{\mathsf{x}} \partial \phi_{b,u,0}} \frac{\partial \phi_{b,u,0}}{\partial p_{u}^{\mathsf{x}}} + \sum_{b=1}^{N_{\mathsf{B}}} \frac{\partial \ell_{u}}{\partial \phi_{b,u,0}} \frac{\partial^{2} \phi_{b,u,0}}{\partial p_{u}^{\mathsf{x}} \partial p_{u}^{\mathsf{x}}} + \sum_{b=1}^{N_{\mathsf{B}}} \frac{\partial^{2} \ell_{u}}{\partial \phi_{b,u,0}} \frac{\partial \phi_{b,u,0}}{\partial p_{u}^{\mathsf{x}}} + \sum_{b=1}^{N_{\mathsf{B}}} \frac{\partial^{2} \ell_{u}}{\partial \theta_{b,u,0}} \frac{\partial^{2} \theta_{b,u,0}}{\partial p_{u}^{\mathsf{x}} \partial p_{u}^{\mathsf{x}}} + \sum_{b=1}^{N_{\mathsf{B}}} \frac{\partial^{2} \ell_{u}}{\partial \theta_{b,u,0}} \frac{\partial^{2} \ell_{b,u}}{\partial p_{u}^{\mathsf{x}} \partial p_{u}^{\mathsf{x}}} + \sum_{b=1}^{N_{\mathsf{B}}} \frac{\partial^{2} \ell_{u}}{\partial r_{b,u}} \frac{\partial^{2} r_{b,u}}{\partial p_{u}^{\mathsf{x}} \partial p_{u}^{\mathsf{x}}}. \quad (58)$$

Other elements of  $\nabla^2 \ell_u$  can also be expressed similarly. In (58),  $\frac{\partial^2 \ell_u}{\partial p_u^x \partial \phi_{b,u,0}}$  can be derived using (53a) as

$$\frac{\partial^{2} \ell_{u}}{\partial p_{u}^{x} \partial \phi_{b,u,0}} = 2\xi_{b,u}^{(L)} \Re \left\{ \sum_{k=1}^{K} \left( \frac{\partial \phi_{b,u,0}}{\partial p_{u}^{x}} \frac{\partial \omega_{\phi,k}}{\partial \phi_{b,u,0}} + \frac{\partial \theta_{b,u,0}}{\partial p_{u}^{x}} \frac{\partial \omega_{\phi,k}}{\partial r_{b,u}} \right) \right\}$$
(59)

where  $\omega_{\phi,k} \triangleq (\tilde{z}_{b,u}^{(1)}[k])^{\dagger} \tilde{\Sigma}_{b,u}^{-1}[k] \frac{\partial \tilde{\mu}_{b,u}^{(1)}[k]}{\partial \phi_{b,u,0}}$ . The derivatives of  $\omega_{\phi,k}$  with respect to  $\phi_{b,u,0}$ ,  $\theta_{b,u,0}$ , and  $r_{b,u}$  can be easily obtained by using the intermediate terms given in the previous subsection. Similarly,  $\frac{\partial^2 \ell_u}{\partial p_u^* \partial \theta_{b,u,0}}$  in (58) can be obtained

using (53b). The term  $\frac{\partial^2 \ell_u}{\partial p_x^{\rm v} \partial r_{b,u}}$  in (58) is given by the derivative of (53c) with respect to  $p_u^{\rm v}$ , where the second derivative of the log of the Gaussian PDF is needed as

$$\frac{\partial^{2}}{\partial p_{u}^{\mathbf{x}} \partial r_{b,u}} \ln \varphi \left( \mathbf{y}_{b,u}[k]; \tilde{\boldsymbol{\mu}}_{b,u}^{(\chi_{b,u})}[k], \tilde{\boldsymbol{\Sigma}}_{b,u}[k] \right) \\
= \frac{\partial \phi_{b,u,0}}{\partial p_{u}^{\mathbf{x}}} \zeta_{\phi,k} + \frac{\partial \theta_{b,u,0}}{\partial p_{u}^{\mathbf{x}}} \zeta_{\theta,k} + \frac{\partial r_{b,u}}{\partial p_{u}^{\mathbf{x}}} \zeta_{r,k} \qquad (60)$$

where

$$\begin{split} \zeta_{\phi,k} &= -2\Re\Big\{ \big(\tilde{\boldsymbol{z}}_{b,u}^{(\chi_{b,u})}[k]\big)^{\dagger} \boldsymbol{X}_{k} \frac{\partial \tilde{\boldsymbol{\mu}}_{b,u}^{(\chi_{b,u})}[k]}{\partial \phi_{b,u,0}} \\ &+ \Big(\frac{\partial \tilde{\boldsymbol{\mu}}_{b,u}^{(\chi_{b,u})}[k]}{\partial \phi_{b,u,0}}\Big)^{\dagger} \tilde{\boldsymbol{\Sigma}}_{b,u}^{-1}[k] \frac{\partial \tilde{\boldsymbol{\mu}}_{b,u}^{(\chi_{b,u})}[k]}{\partial r_{b,u}} \\ &- \big(\tilde{\boldsymbol{z}}_{b,u}^{(\chi_{b,u})}[k]\big)^{\dagger} \tilde{\boldsymbol{\Sigma}}_{b,u}^{-1}[k] \frac{\partial^{2} \tilde{\boldsymbol{\mu}}_{b,u}^{(\chi_{b,u})}[k]}{\partial \phi_{b,u,0} \partial r_{b,u}} \Big\} \\ \zeta_{\theta,k} &= -2\Re\Big\{ \Big(\tilde{\boldsymbol{z}}_{b,u}^{(\chi_{b,u})}[k]\Big)^{\dagger} \boldsymbol{X}_{k} \frac{\partial \tilde{\boldsymbol{\mu}}_{b,u}^{(\chi_{b,u})}[k]}{\partial \theta_{b,u,0}} \\ &+ \Big(\frac{\partial \tilde{\boldsymbol{\mu}}_{b,u}^{(\chi_{b,u})}[k]}{\partial \theta_{b,u,0}}\Big)^{\dagger} \tilde{\boldsymbol{\Sigma}}_{b,u}^{-1}[k] \frac{\partial \tilde{\boldsymbol{\mu}}_{b,u}^{(\chi_{b,u})}[k]}{\partial r_{b,u}} \Big\} \\ &- \Big(\tilde{\boldsymbol{z}}_{b,u}^{(\chi_{b,u})}[k]\Big)^{\dagger} \tilde{\boldsymbol{\Sigma}}_{b,u}^{-1}[k] \frac{\partial^{2} \tilde{\boldsymbol{\mu}}_{b,u}^{(\chi_{b,u})}[k]}{\partial \theta_{b,u,0} \partial r_{b,u}} \Big\} \\ \zeta_{r,k} &= \operatorname{tr}\Big(\frac{\beta_{N}}{r_{b,u}^{2}}\Big((\beta_{N}-1)P_{n}\tilde{\boldsymbol{\Sigma}}_{b,u}^{-1}[k] + \beta_{N}P_{n}^{2}\tilde{\boldsymbol{\Sigma}}_{b,u}^{-2}[k] - \boldsymbol{I}\Big)\Big) \\ &- 2\Re\Big\{\Big(\tilde{\boldsymbol{z}}_{b,u}^{(\chi_{b,u})}[k]\Big)^{\dagger} \boldsymbol{X}_{k} \frac{\partial \tilde{\boldsymbol{\mu}}_{b,u}^{(\chi_{b,u})}[k]}{\partial r_{b,u}}\Big\} \Big\} \\ &- \frac{\beta_{N}(1+\beta_{N})}{r_{b,u}^{2}}\Big(\tilde{\boldsymbol{z}}_{b,u}^{(\chi_{b,u})}[k]\Big)^{\dagger} \Big(\tilde{\boldsymbol{\Sigma}}_{b,u}^{-1}[k] - P_{n}\tilde{\boldsymbol{\Sigma}}_{b,u}^{-2}[k]\Big)\tilde{\boldsymbol{z}}_{b,u}^{(\chi_{b,u})}[k] \\ &+ 2\Re\Big\{-\Big(\frac{\partial \tilde{\boldsymbol{\mu}}_{b,u}^{(\chi_{b,u})}[k]}{\partial r_{b,u}}\Big)^{\dagger} \tilde{\boldsymbol{\Sigma}}_{b,u}^{-1}[k] + \tilde{\boldsymbol{\Sigma}}_{b,u}^{-1}[k] \frac{\partial^{2} \tilde{\boldsymbol{\mu}}_{b,u}^{(\chi_{b,u})}[k]}{\partial r_{b,u}}\Big\} \Big\} \\ &+ \Big(\tilde{\boldsymbol{z}}_{b,u}^{(\chi_{b,u})}[k]\Big)^{\dagger}\Big(-\boldsymbol{X}_{k}\frac{\partial \tilde{\boldsymbol{\mu}}_{b,u}^{(\chi_{b,u})}[k]}{\partial r_{b,u}} + \tilde{\boldsymbol{\Sigma}}_{b,u}^{-1}[k]\frac{\partial^{2} \tilde{\boldsymbol{\mu}}_{b,u}^{(\chi_{b,u})}[k]}{\partial r_{b,u}\partial r_{b,u}}\Big) \Big\} \end{aligned}$$

where  $X_k \triangleq \tilde{\Sigma}_{b,u}^{-1}[k] \frac{\partial \tilde{\Sigma}_{b,u}[k]}{\partial r_{b,u}} \tilde{\Sigma}_{b,u}^{-1}[k]$ . The second derivatives of  $\ln p_{\rm L}(r_{b,u})$  and  $\ln (1-p_{\rm L}(r_{b,u}))$  can also be easily obtained. The remaining terms in (58) can be obtained using (41a), (41b), and (56).

## REFERENCES

- Service Requirements for the 5G System; Stage 1 (Release 19), 3GPP Technical Specification Group Services System Aspects, document TS 22.261, V19.1.0, Dec. 2022.
- [2] A. Conti et al., "Location awareness in beyond 5G networks," *IEEE Commun. Mag.*, vol. 59, no. 11, pp. 22–27, Nov. 2021.
- [3] Study on NR Positioning Support (Release 16), 3GPP Technical Specification Group Radio Access Network, document TR 38.855, V16.0.0, Mar. 2019.
- [4] F. Morselli, S. M. Razavi, M. Z. Win, and A. Conti, "Soft information based localization for 5G networks and beyond," *IEEE Trans. Wireless Commun.*, vol. 22, pp. 1–16, 2023.
- [5] Study on NR Positioning Enhancements (Release 17), 3GPP Technical Specification Group Radio Access Network, document TR 38.857, V17.0.0, Mar. 2021.

- [6] G. Torsoli, M. Z. Win, and A. Conti, "Blockage intelligence in complex environments for beyond 5G localization," *IEEE J. Sel. Areas Commun.*, vol. 41, no. 6, pp. 1688–1701, Jun. 2023.
- [7] F. Bai, H. Krishnan, T. Elbatt, and G. Holland, "Towards characterising and classifying communication-based automotive applications from a wireless networking perspective," *Int. J. Vehicle Auton. Syst.*, vol. 10, no. 3, pp. 165–197, Jan. 2013.
- [8] G. Bresson, Z. Alsayed, L. Yu, and S. Glaser, "Simultaneous localization and mapping: A survey of current trends in autonomous driving," *IEEE Trans. Intell. Vehicles*, vol. 2, no. 3, pp. 194–220, Sep. 2017.
- [9] J. Thomas, J. Welde, G. Loianno, K. Daniilidis, and V. Kumar, "Autonomous flight for detection, localization, and tracking of moving targets with a small quadrotor," *IEEE Robot. Autom. Lett.*, vol. 2, no. 3, pp. 1762–1769, Jul. 2017.
- [10] D. Wu, D. Chatzigeorgiou, K. Youcef-Toumi, and R. Ben-Mansour, "Node localization in robotic sensor networks for pipeline inspection," *IEEE Trans. Ind. Informat.*, vol. 12, no. 2, pp. 809–819, Apr. 2016.
- [11] N. Cordeschi, D. Amendola, and E. Baccarelli, "Reliable adaptive resource management for cognitive cloud vehicular networks," *IEEE Trans. Veh. Technol.*, vol. 64, no. 6, pp. 2528–2537, Jun. 2015.
- [12] S. Bartoletti, A. Conti, and M. Z. Win, "Device-free counting via wideband signals," *IEEE J. Sel. Areas Commun.*, vol. 35, no. 5, pp. 1163–1174, May 2017.
- [13] J. Chen, D. K. Grimm, F. Bai, J. Grace, S. Relan, and W. Vavrik, "Crowd-sensing road surface quality using connected vehicle data," *Transp. Res. Rec.*, J. Transp. Res. Board, vol. 2675, no. 11, pp. 729–739, Nov. 2021.
- [14] C. Zhu, Y.-H. Chiang, Y. Xiao, and Y. Ji, "FlexSensing: A QoI and latency-aware task allocation scheme for vehicle-based visual crowdsourcing via deep Q-network," *IEEE Internet Things J.*, vol. 8, no. 9, pp. 7625–7637, May 2021.
- [15] F. Zabini and A. Conti, "Inhomogeneous Poisson sampling of finite-energy signals with uncertainties in R<sup>d</sup>," *IEEE Trans. Signal Process.*, vol. 64, no. 18, pp. 4679–4694, Sep. 2016.
- [16] K. Lin, M. Chen, J. Deng, M. M. Hassan, and G. Fortino, "Enhanced fingerprinting and trajectory prediction for IoT localization in smart buildings," *IEEE Trans. Autom. Sci. Eng.*, vol. 13, no. 3, pp. 1294–1307, Jul 2016
- [17] D. Dardari, A. Conti, C. Buratti, and R. Verdone, "Mathematical evaluation of environmental monitoring estimation error through energyefficient wireless sensor networks," *IEEE Trans. Mobile Comput.*, vol. 6, no. 7, pp. 790–802, Jul. 2007.
- [18] V. Moreno, M. A. Zamora, and A. F. Skarmeta, "A low-cost indoor localization system for energy sustainability in smart buildings," *IEEE Sensors J.*, vol. 16, no. 9, pp. 3246–3262, May 2016.
- [19] M. Chiani, A. Giorgetti, and E. Paolini, "Sensor radar for object tracking," Proc. IEEE, vol. 106, no. 6, pp. 1022–1041, Jun. 2018.
- [20] K. Witrisal et al., "High-accuracy localization for assisted living: 5G systems will turn multipath channels from foe to friend," *IEEE Signal Process. Mag.*, vol. 33, no. 2, pp. 59–70, Mar. 2016.
- [21] J. Werb and C. Lanzl, "Designing a positioning system for finding things and people indoors," *IEEE Spectr.*, vol. 35, no. 9, pp. 71–78, Sep. 1998.
- [22] F. Meyer et al., "Message passing algorithms for scalable multitarget tracking," *Proc. IEEE*, vol. 106, no. 2, pp. 221–259, Feb. 2018.
- [23] M. Z. Win, F. Meyer, Z. Liu, W. Dai, S. Bartoletti, and A. Conti, "Efficient multi-sensor localization for the Internet of Things," *IEEE Signal Process. Mag.*, vol. 35, no. 5, pp. 153–167, Sep. 2018.
- [24] S. D'Oro, L. Galluccio, G. Morabito, and S. Palazzo, "Exploiting object group localization in the Internet of Things: Performance analysis," *IEEE Trans. Veh. Technol.*, vol. 64, no. 8, pp. 3645–3656, Aug. 2015.
- Trans. Veh. Technol., vol. 64, no. 8, pp. 3645–3656, Aug. 2015.
  [25] S. G. Nagarajan, P. Zhang, and I. Nevat, "Geo-spatial location estimation for Internet of Things (IoT) networks with one-way time-of-arrival via stochastic censoring," IEEE Internet Things J., vol. 4, no. 1, pp. 205–214, Feb. 2017.
- [26] F. De Rango, M. Tropea, A. Serianni, and N. Cordeschi, "Fuzzy inference system design for promoting an eco-friendly driving style in IoV domain," Veh. Commun., vol. 34, Apr. 2022, Art. no. 100415.
- [27] C-V2X Use Cases and Service Level Requirements, 5G Automot. Assoc. (5GAA), Munich, Germany, Dec. 2020.
- [28] J. Choi, V. Va, N. Gonzalez-Prelcic, R. Daniels, C. R. Bhat, and R. W. Heath, "Millimeter-wave vehicular communication to support massive automotive sensing," *IEEE Commun. Mag.*, vol. 54, no. 12, pp. 160–167, Dec. 2016.

- [29] J. A. del Peral-Rosado, R. Raulefs, J. A. López-Salcedo, and G. Seco-Granados, "Survey of cellular mobile radio localization methods: From 1G to 5G," *IEEE Commun. Surveys Tuts.*, vol. 20, no. 2, pp. 1124–1148, 2nd Quart., 2018.
- [30] A. Behravan et al., "Positioning and sensing in 6G: Gaps, challenges, and opportunities," *IEEE Veh. Technol. Mag.*, vol. 18, no. 1, pp. 40–48, Mar. 2023.
- [31] J. G. Andrews et al., "What will 5G be?" IEEE J. Sel. Areas Commun., vol. 32, no. 6, pp. 1065–1082, Jun. 2014.
- [32] M. Z. Win, Z. Wang, Z. Liu, Y. Shen, and A. Conti, "Location awareness via intelligent surfaces: A path toward holographic NLN," *IEEE Veh. Technol. Mag.*, vol. 17, no. 2, pp. 37–45, Jun. 2022.
- [33] R. W. Heath, N. González-Prelcic, S. Rangan, W. Roh, and A. M. Sayeed, "An overview of signal processing techniques for millimeter wave MIMO systems," *IEEE J. Sel. Topics Signal Process.*, vol. 10, no. 3, pp. 436–453, Apr. 2016.
- [34] O. E. Ayach, S. Rajagopal, S. Abu-Surra, Z. Pi, and R. W. Heath, "Spatially sparse precoding in millimeter wave MIMO systems," *IEEE Trans. Wireless Commun.*, vol. 13, no. 3, pp. 1499–1513, Mar. 2014.
- [35] K. Venugopal, A. Alkhateeb, N. González Prelcic, and R. W. Heath, "Channel estimation for hybrid architecture-based wideband millimeter wave systems," *IEEE J. Sel. Areas Commun.*, vol. 35, no. 9, pp. 1996–2009, Sep. 2017.
- [36] G. Kwon, N. Kim, and H. Park, "Millimeter wave SDMA with limited feedback: RF-only beamforming can outperform hybrid beamforming," *IEEE Trans. Veh. Technol.*, vol. 68, no. 2, pp. 1534–1548, Feb. 2019.
- [37] S. He et al., "A survey of millimeter-wave communication: Physical-layer technology specifications and enabling transmission technologies," *Proc. IEEE*, vol. 109, no. 10, pp. 1666–1705, Oct. 2021.
- [38] G. Kwon and H. Park, "Limited feedback hybrid beamforming for multi-mode transmission in wideband millimeter wave channel," *IEEE Trans. Wireless Commun.*, vol. 19, no. 6, pp. 4008–4022, Jun. 2020.
- [39] A. Kakkavas, M. H. C. García, R. A. Stirling-Gallacher, and J. A. Nossek, "Performance limits of single-anchor millimeterwave positioning," *IEEE Trans. Wireless Commun.*, vol. 18, no. 11, pp. 5196–5210, Nov. 2019.
- [40] A. Guerra, F. Guidi, and D. Dardari, "Single-anchor localization and orientation performance limits using massive arrays: MIMO vs. beamforming," *IEEE Trans. Wireless Commun.*, vol. 17, no. 8, pp. 5241–5255, Aug. 2018.
- [41] Z. Abu-Shaban, X. Zhou, T. Abhayapala, G. Seco-Granados, and H. Wymeersch, "Error bounds for uplink and downlink 3D localization in 5G millimeter wave systems," *IEEE Trans. Wireless Commun.*, vol. 17, no. 8, pp. 4939–4954, Aug. 2018.
- [42] Z. Wang, Z. Liu, Y. Shen, A. Conti, and M. Z. Win, "Location awareness in beyond 5G networks via reconfigurable intelligent surfaces," *IEEE J. Sel. Areas Commun.*, vol. 40, no. 7, pp. 2011–2025, Jul. 2022.
- [43] G. Kwon, A. Conti, H. Park, and M. Z. Win, "Joint communication and localization in millimeter wave networks," *IEEE J. Sel. Topics Signal Process.*, vol. 15, no. 6, pp. 1439–1454, Nov. 2021.
- [44] M. F. Keskin, F. Jiang, F. Munier, G. Seco-Granados, and H. Wymeersch, "Optimal spatial signal design for mmWave positioning under imperfect synchronization," *IEEE Trans. Veh. Technol.*, vol. 71, no. 5, pp. 5558–5563, May 2022.
- [45] X. Cui, T. A. Gulliver, J. Li, and H. Zhang, "Vehicle positioning using 5G millimeter-wave systems," *IEEE Access*, vol. 4, pp. 6964–6973, 2016.
- [46] Z. Lin, T. Lv, and P. T. Mathiopoulos, "3-D indoor positioning for millimeter-wave massive MIMO systems," *IEEE Trans. Commun.*, vol. 66, no. 6, pp. 2472–2486, Jun. 2018.
- [47] J. Palacios, G. Bielsa, P. Casari, and J. Widmer, "Single- and multiple-access point indoor localization for millimeter-wave networks," *IEEE Trans. Wireless Commun.*, vol. 18, no. 3, pp. 1927–1942, Mar. 2019.
- [48] W. Wang and W. Zhang, "Joint beam training and positioning for intelligent reflecting surfaces assisted millimeter wave communications," *IEEE Trans. Wireless Commun.*, vol. 20, no. 10, pp. 6282–6297, Oct. 2021.

- [49] A. Fascista, A. Coluccia, H. Wymeersch, and G. Seco-Granados, "Millimeter-wave downlink positioning with a single-antenna receiver," *IEEE Trans. Wireless Commun.*, vol. 18, no. 9, pp. 4479–4490, Sep. 2019.
- [50] D. Dardari, A. Conti, U. Ferner, A. Giorgetti, and M. Z. Win, "Ranging with ultrawide bandwidth signals in multipath environments," *Proc. IEEE*, vol. 97, no. 2, pp. 404–426, Feb. 2009.
- [51] L. Cong and W. Zhuang, "Hybrid TDOA/AOA mobile user location for wideband CDMA cellular systems," *IEEE Trans. Wireless Commun.*, vol. 1, no. 3, pp. 439–447, Jul. 2002.
- [52] L. Cong and W. Zhuang, "Nonline-of-sight error mitigation in mobile location," *IEEE Trans. Wireless Commun.*, vol. 4, no. 2, pp. 560–573, Mar. 2005.
- [53] U. A. Khan, S. Kar, and J. M. F. Moura, "Distributed sensor localization in random environments using minimal number of anchor nodes," *IEEE Trans. Signal Process.*, vol. 57, no. 5, pp. 2000–2016, May 2009.
- [54] U. A. Khan, S. Kar, and J. M. F. Moura, "DILAND: An algorithm for distributed sensor localization with noisy distance measurements," *IEEE Trans. Signal Process.*, vol. 58, no. 3, pp. 1940–1947, Mar. 2010.
- [55] A. J. Weiss, "Direct position determination of narrowband radio frequency transmitters," *IEEE Signal Process. Lett.*, vol. 11, no. 5, pp. 513–516, May 2004.
- [56] N. Vankayalapati, S. Kay, and Q. Ding, "TDOA based direct positioning maximum likelihood estimator and the cramer-rao bound," *IEEE Trans. Aerosp. Electron. Syst.*, vol. 50, no. 3, pp. 1616–1635, Jul. 2014.
- [57] L. Tzafri and A. J. Weiss, "High-resolution direct position determination using MVDR," *IEEE Trans. Wireless Commun.*, vol. 15, no. 9, pp. 6449–6461, Sep. 2016.
- [58] O. Bialer, D. Raphaeli, and A. J. Weiss, "Maximum-likelihood direct position estimation in dense multipath," *IEEE Trans. Veh. Technol.*, vol. 62, no. 5, pp. 2069–2079, Jun. 2013.
- [59] Z. Lu, J. Wang, B. Ba, and D. Wang, "A novel direct position determination algorithm for orthogonal frequency division multiplexing signals based on the time and angle of arrival," *IEEE Access*, vol. 5, pp. 25312–25321, 2017.
- [60] A. Conti, S. Mazuelas, S. Bartoletti, W. C. Lindsey, and M. Z. Win, "Soft information for localization-of-things," *Proc. IEEE*, vol. 107, no. 11, pp. 2240–2264, Nov. 2019.
- [61] D. C. Mur, A. Gavras, M. Ghoraishi, H. Hrasnica, and A. Kaloxylos, "AI and ML-enablers for beyond 5G networks," 5G Infrastruct. Public Private Partnership (5G PPP), West-Vlaanderen, Belgium, Version is 1.0, May 2021. [Online]. Available: https://5g-ppp.eu/wpcontent/uploads/2021/05/AI-MLforNetworks-v1-0.pdf
- [62] Study on Channel Model for Frequencies From 0.5 to 100 GHz (Release 16), 3GPP Technical Specification Group Radio Access Network, document TR 38.901 (V16.1.0), Dec. 2019.
- [63] M. Steinbauer, A. F. Molisch, and E. Bonek, "The double-directional radio channel," *IEEE Antennas Propag. Mag.*, vol. 43, no. 4, pp. 51–63, Aug. 2001.
- [64] S. Buzzi, C. D'Andrea, D. Li, and S. Feng, "MIMO-UFMC transceiver schemes for millimeter-wave wireless communications," *IEEE Trans. Commun.*, vol. 67, no. 5, pp. 3323–3336, May 2019.
- [65] J. P. González-Coma, J. Rodríguez-Fernández, N. González-Prelcic, L. Castedo, and R. W. Heath, "Channel estimation and hybrid precoding for frequency selective multiuser mmWave MIMO systems," *IEEE J. Sel. Topics Signal Process.*, vol. 12, no. 2, pp. 353–367, May 2018.
- [66] R. Miller and C. Chang, "A modified Cramér-Rao bound and its applications (corresp)," *IEEE Trans. Inf. Theory*, vol. IT-24, no. 3, pp. 398–400, May 1978.
- [67] D. P. Bertsekas, Nonlinear Programming, 3rd ed. Belmont, MA, USA: Athena Scientific, 2016.
- [68] C. F. J. Wu, "On the convergence properties of the EM algorithm," Ann. Statist., vol. 11, no. 1, pp. 95–103, Mar. 1983.
- [69] G. Golub and C. V. Loan, *Matrix Computations*, 3rd ed. Baltimore, MD, USA: The Johns Hopkins Univ. Press, 1996.
- [70] M. L. Eaton, Multivariate Statistics: A Vector Space Approach. New York, NY, USA: Wiley, 1983.
- [71] M. Radaelli, G. T. Landi, K. Modi, and F. C. Binder, "Fisher information of correlated stochastic processes," 2022, arXiv:2206.00463v1.
- [72] S. M. Kay, Fundamentals of Statistical Signal Processing: Estimation Theory. Upper Saddle River, NJ, USA: Prentice-Hall, 1993.



Girim Kwon (Member, IEEE) received the B.S. degree (with the highest honor) in electrical engineering from the University of Seoul, Seoul, South Korea, in 2013, and the M.S. and Ph.D. degrees in electrical engineering from the Korea Advanced Institute of Science and Technology (KAIST), Daejeon, South Korea, in 2014 and 2020, respectively.

He is currently a Postdoctoral Fellow with the Wireless Information and Network Sciences Laboratory at the Massachusetts Institute of Technology,

Cambridge, MA, USA. His current research interests include wireless communications, network localization and navigation, satellite networks, and machine learning.

Dr. Kwon was a recipient of the S-Oil Best Dissertation Award in 2021, the Best Ph.D. Dissertation Award from KAIST in 2020, the ICT Paper Award from the Electronic Times in 2018, and the Global Ph.D. Fellowship from the Korean Government in 2015.



**Zhenyu Liu** (Member, IEEE) received the B.S. (Hons.) and M.S. degrees in electronic engineering from Tsinghua University, Beijing, China, in 2011 and 2014, respectively, and the S.M. degree in aeronautics and astronautics and the Ph.D. degree in networks and statistics from the Massachusetts Institute of Technology (MIT) in 2022.

Since 2022, he has been a Postdoctoral Associate in the Wireless Information and Network Sciences Laboratory at MIT. His research interests include wireless communications, network localization, dis-

tributed inference, networked control, and quantum information science.

Dr. Liu received the first prize in the IEEE Communications Society's Student Competition in 2016 and 2019, the R&D 100 Award for Peregrine Systems in 2018, and the Best Paper Award at the IEEE Latin-American Conference on Communications in 2017.



Andrea Conti (Fellow, IEEE) is a Professor and founding director of the Wireless Communication and Localization Networks Laboratory at the University of Ferrara, Italy. Prior to joining the University of Ferrara, he was with CNIT and with IEIT-CNR.

In Summer 2001, he was with the Wireless Systems Research Department at AT&T Research Laboratories. Since 2003, he has been a frequent visitor with the Wireless Information and Network Sciences Laboratory at the Massachusetts Institute

of Technology, where he presently holds the Research Affiliate appointment. His research interests involve the theory and experimentation of wireless communication and localization systems. His current research topics include network localization and navigation, distributed sensing, adaptive diversity communications, and quantum information science.

Dr. Conti has served as editor for IEEE journals and chaired international conferences. He was elected Chair of the IEEE Communications Society's Radio Communications Technical Committee and is Co-founder of the IEEE Quantum Communications and Information Technology Emerging Technical Subcommittee. He received the HTE Puskás Tivadar Medal, the IEEE Communications Society's Fred W. Ellersick Prize, and the IEEE Communications Society's Stephen O. Rice Prize in the field of Communications Theory. He is an elected Fellow of the IET and a member of Sigma Xi. He has been selected as an IEEE Distinguished Lecturer.



**Hyuncheol Park** (Senior Member, IEEE) received the B.S. and M.S. degrees in electronics engineering from Yonsei University, Seoul, South Korea, in 1983 and 1985, respectively, and the Ph.D. degree in electrical engineering from the Georgia Institute of Technology, Atlanta, GA, USA, in 1997.

He was a Senior Engineer from 1985 to 1991 and a Principal Engineer from 1997 to 2002 with Samsung Electronics Company Ltd., South Korea. Since 2002, he has been with the School of Electrical Engineering, Korea Advanced Institute of Science

and Technology, Daejeon, South Korea, where he is currently a Professor. His research interests include communication theory and machine learning.



Moe Z. Win (Fellow, IEEE) is a Professor at the Massachusetts Institute of Technology (MIT) and the founding director of the Wireless Information and Network Sciences Laboratory. Prior to joining MIT, he was with AT&T Research Laboratories and the NASA Jet Propulsion Laboratory.

His research encompasses fundamental theories, algorithm design, and network experimentation for a broad range of real-world problems. His current research topics include ultra-wideband systems, network localization and navigation, network inter-

ference exploitation, and quantum information science. He has served the IEEE Communications Society as an elected Member-at-Large on the Board of Governors, as elected Chair of the Radio Communications Committee, and as an IEEE Distinguished Lecturer. Over the last two decades, he held various editorial positions for IEEE journals and organized numerous international conferences. Recently, he served on the SIAM Diversity Advisory Committee.

Dr. Win is an elected Fellow of the AAAS, the EURASIP, and the IET. He was honored with two IEEE Technical Field Awards: the IEEE Kiyo Tomiyasu Award (2011) and the IEEE Eric E. Sumner Award (2006, jointly with R. A. Scholtz). His publications, co-authored with students and colleagues, have received several awards. Other recognitions include the MIT Everett Moore Baker Award (2022), the IEEE Vehicular Technology Society James Evans Avant Garde Award (2022), the IEEE Communications Society Edwin H. Armstrong Achievement Award (2016), the Cristoforo Colombo International Prize for Communications (2013), the Copernicus Fellowship (2011) and the *Laurea Honoris Causa* (2008) both from the Università degli Studi di Ferrara, and the U.S. Presidential Early Career Award for Scientists and Engineers (2004). He is an ISI Highly Cited Researcher.